



<http://www.diva-portal.org>

This is the published version of a paper published in *Medical physics (Lancaster)*.

Citation for the original published paper (version of record):

Andersson, J., Bednarek, D R., Bolch, W., Boltz, T., Bosmans, H. et al. (2021)
Estimation of patient skin dose in fluoroscopy: summary of a joint report by AAPM
TG357 and EFOMP
Medical physics (Lancaster), 48(7): e671-e696
<https://doi.org/10.1002/mp.14910>

Access to the published version may require subscription.

N.B. When citing this work, cite the original published paper.

Permanent link to this version:

<http://urn.kb.se/resolve?urn=urn:nbn:se:umu:diva-183708>

Estimation of patient skin dose in fluoroscopy: summary of a joint report by AAPM TG357 and EFOMP

Jonas Andersson^{a)}

Department of Radiation Sciences, Radiation Physics, Umeå University, SE-901 85 Umeå, Sweden

Daniel R. Bednarek

State University of New York, 875 Ellicott St, Buffalo, NY 14203-1070, USA

Wesley Bolch

University of Florida, 1275 Center Drive, Gainesville, FL 32611-6131, USA

Thomas Boltz

Orange Factor Imaging Physicists, 4035 E Captain Dreyfus Ave, Phoenix, AZ 85032, USA

Hilde Bosmans

University of Leuven, Herestraat 49, Leuven B-3000, Belgium

Amber J. Gislason-Lee

University of Leeds, Worsley Building, Clarendon Way, Leeds LS2 9JT, UK

Christoffer Granberg and Max Hellstrom

Department of Radiation Sciences, Radiation Physics, Umeå University, SE-901 85 Umeå, Sweden

Kalpana Kanal

University of Washington Medical Center, 1959 NE Pacific Street, Seattle, WA 98195, USA

Ed McDonagh

Joint Department of Physics, The Royal Marsden NHS Foundation Trust, Fulham Road, London SW3 6JJ, UK

Robert Paden

Mayo Clinic, 5777 East Mayo Blvd, Phoenix, AZ 85054, USA

William Pavlicek

Mayo Clinic, 13400 E Shea Blvd., Scottsdale, AZ 85259, USA

Yasaman Khodadadegan

Progressive Insurance, Customer Relation Management, 6300 Wilson Mills Rd., Mayfield Village, OH 44143, USA

Alberto Torresin

Niguarda Ca'Granda Hospital, Via Leon Battista Alberti 5, Milano 20149, Italy

Annalisa Trianni

Udine University Hospital, Piazzale S. Maria Della Misericordia, n. 15, 33100 Udine, Italy

David Zamora

University of Washington Medical Center, 6852 31st Ave NE, Seattle, WA 98115-7245, USA

(Received 3 January 2021; revised 4 April 2021; accepted for publication 23 April 2021; published 20 May 2021)

Background: Physicians use fixed C-arm fluoroscopy equipment with many interventional radiological and cardiological procedures. The associated effective dose to a patient is generally considered low risk, as the benefit-risk ratio is almost certainly highly favorable. However, X-ray-induced skin injuries may occur due to high absorbed patient skin doses from complex fluoroscopically guided interventions (FGI). Suitable action levels for patient-specific follow-up could improve the clinical practice.

There is a need for a refined metric regarding follow-up of X-ray-induced patient injuries and the knowledge gap regarding skin dose-related patient information from fluoroscopy devices must be filled. The most useful metric to indicate a risk of erythema, epilation or greater skin injury that also includes actionable information is the peak skin dose, that is, the largest dose to a region of skin.

Materials and Methods: The report is based on a comprehensive review of best practices and methods to estimate peak skin dose found in the scientific literature and situates the importance of the Digital Imaging and Communication in Medicine (DICOM) standard detailing pertinent information contained in the Radiation Dose Structured Report (RDSR) and DICOM image headers for FGI devices. Furthermore, the expertise of the task group members and consultants have been used to bridge and discuss different methods and associated available DICOM information for peak skin dose estimation.

Results: The report contributes an extensive summary and discussion of the current state of the art in estimating peak skin dose with FGI procedures with regard to methodology and DICOM information. Improvements in skin dose estimation efforts with more refined DICOM information are suggested and discussed.

Conclusions: The endeavor of skin dose estimation is greatly aided by the continuing efforts of the scientific medical physics community, the numerous technology enhancements, the dose-controlling features provided by the FGI device manufacturers, and the emergence and greater availability of the DICOM RDSR. Refined and new dosimetry systems continue to evolve and form the infrastructure for further improvements in accuracy. Dose-related content and information systems capable of handling big data are emerging for patient dose monitoring and quality assurance tools for large-scale multihospital enterprises. © 2021 The Authors. *Medical Physics* published by Wiley Periodicals LLC on behalf of American Association of Physicists in Medicine [https://doi.org/10.1002/mp.14910]

Key words: x-ray fluoroscopy, peak skin dose, fluoroscopically guided interventions

1. INTRODUCTION

Physicians use fixed C-arm fluoroscopy equipment with many interventional radiological procedures. The associated effective dose to a patient with fluoroscopic and interventional procedures is generally considered low risk, as the benefit-risk ratio is almost certainly highly favorable. However, X-ray-induced skin injuries may occur due to high absorbed patient skin doses from complex fluoroscopically guided interventions (FGI) requiring suitable action levels for patient-specific follow-up. Metrics such as fluoroscopy time, air kerma-area product, or the number of digital subtraction angiography (DSA) runs have historically been used for radiation monitoring of patient exposure. These metrics lack correlation to X-ray beam quality, variable pulse rates, dose rates, patient size and the geometrical factors that greatly influence skin dose. Despite these limitations, regulatory and accrediting bodies do require the capture and the review of fluoroscopic time, as it can relate to personal practice preferences of physicians. A directly available metric for quality assurance (QA) of patient dose is the cumulative air kerma. This exposure value is referenced to a specific location, the patient entrance reference point (PERP). This reference point is located along the central X-ray beam, commonly but not always at a distance of 15 cm from the isocenter in the direction of the X-ray tube. The cumulative air kerma is available on most interventional C-arm X-ray equipment since 2006, when it became mandated by the FDA.¹ However, the cumulative air kerma also has known limitations as a predictor of patient peak skin dose (PSD). Miller *et al.* found that the cumulative air kerma overstated the PSD by 40%–50% and thus cumulative air kerma for a procedure likely represents a conservative surrogate index of PSD for QA reviews.² However, Miller *et al.* also showed the possibility that the tabletop height and image receptor positioning can be such that the cumulative air kerma actually underestimates the PSD received by a patient.²

There is a need for a refined metric regarding follow-up of X-ray-induced patient injuries and the knowledge gap regarding skin dose-related patient information from fluoroscopy devices must be filled. The most useful metric to indicate a

risk of erythema, epilation or greater skin injury that also include actionable information is the PSD, which gives the largest dose to a region of skin.

Recently the International Electrotechnical Commission (IEC) stated the importance of skin dose estimation and skin dose mapping by including the concepts in the second amendment of IEC 60601-2-43 (“Particular requirements for the basic safety and essential performance of X-ray equipment for interventional procedures”). Here, the IEC made the difference between air kerma mapping and skin dose mapping very clear.³

The American Medical Association, in 2021, has recognized both the importance and complexity of skin dose determinations by specifically defining the medical procedure “Medical physics dose evaluation for radiation exposure that exceeds institutional review threshold, including report”, CPT® 76145. This code will be used by Medical Physicists in the US to report their work in determining absorbed dose to skin (or other organ) subsequent to high dose interventional imaging procedures.

1.A. Purpose and overview

The purpose of this report is (a) to summarize the current state of the art in estimating patient skin doses from fluoroscopic procedures and (b) to outline a road map regarding estimation of PSD from fluoroscopic procedures. To address these purposes, the report includes a comprehensive discussion of (a) the various metrics, concepts, and methods that may be used to achieve estimates of skin dose and (b) the Digital Imaging and Communication in Medicine (DICOM) standard and Radiation Dose Structured Report (RDSR) for FGI devices.

1.B. An open-source framework for discussion and evaluation of skin dose

Compared to other X-ray modalities, the greatest challenge in estimating patient dose metrics may be found for C-arm fluoroscopy equipment, particularly for FGI procedures. This is due to complex geometries, accuracy in representing

patient position and dealing with uncertainty in metrics. There are many different solutions that can be used for estimating skin dose, including commercial, non-commercial and open-source.⁴⁻⁶ To facilitate an in-depth discussion of skin dose estimation, the report uses an open-source framework familiar to the authors that reads RDSR files and, based on the present literature, makes it possible to show clear examples of challenges and solutions.

PySkinDose, an open-source Python™ package for RDSR-based skin dose estimation is used throughout this report as a source of practical examples.^{7,8} This system translates air kerma at the PERP to estimate entrance skin dose for all irradiated surfaces on computational phantoms. The phantoms are oriented with the X-ray source by geometric parameters found within the RDSR, and conversion from air Kerma at the PERP to skin dose is further supported by correction factors found in literature, as well as a limited number of in-clinic measurements, which are discussed in this report (e.g., validation of the coordinate system, table and pad transmission etc.).^{7,8} The output of the software is an estimation of skin dose and a visual indication of skin dose distribution mapped onto an anthropomorphic or a cylindrical phantom. The real position of the phantom on the tabletop can be taken into account. A variety of voxelized phantoms can be incorporated in PySkinDose.

There are many available software solutions for skin dose estimation (both commercial and in-house custom developed), which are also discussed in this report, but the strength of PySkinDose is the open-source format that makes it a good choice for a transparent discussion on models for estimating skin dose together with DICOM information.

1.C. Out of scope

While this report can be useful for all fluoroscopy devices, the focus of this report is fluoroscopic devices with flat panel digital detectors in a basic C-arm configuration. In particular, this report emphasizes those devices used with FGI configured as a C-arm with a fixed isocenter relative to the X-ray tube, an adjustable distance from the X-ray tube to the image receptor, and a patient support system (tabletop) with independent motion.

1.C.1. Organ dose

The aim of this report addresses the immediate need for accurate estimates of PSD. However, it is recognized that organ dose determined from fluoroscopic procedures is a logical next step, and further discussion on this topic may, for example, be found in a publication by Omar et al., which outlines an approach for organ dosimetry with fluoroscopy.⁹

1.C.2. Effective dose

The effective dose (E) is generally expressed for a “standard size” patient. Thus, the effective dose is not a measure

of the dose to an individual patient and effective dose should not be used to estimate or assign individual risk.¹⁰ Since this report has the medical physicist as its target audience and individual patient skin dose as the subject, discussion of the effective dose is out of scope.

2. CURRENT DOSIMETRY METRICS AND ASSOCIATED DICOM INFORMATION

2.A. The Air Kerma and Air Kerma-Area Product (KAP)

Kerma (K) is defined as a ratio of the sum of the initial kinetic energies of all the charged particles liberated by uncharged particles to a mass of material and the unit of kerma is J/kg, or gray (Gy).^{11,12} In medical imaging involving X rays, the kerma is usually expressed in air, that is, air kerma (K_a), which for a monochromatic beam is the product of the energy fluence (ψ) and the mass energy-transfer coefficient for air, $(\mu_{tr}/\rho)_a$.¹³

$$K_a = (\psi \mu_{tr}/\rho)_a. \quad (1)$$

The kerma for a polychromatic beam is the integral of this equation, weighted by the spectral distribution of the X-ray beam energy fluence.

The air kerma-area product (P_{KA}) is the air kerma summed over the radiation field in the plane perpendicular to the beam axis. The displayed units of P_{KA} are commonly Gy·cm², but may vary with manufacturer, type of equipment, and software version, including μGy·m², mGy·cm², cGy·cm², dGy·cm².

P_{KA} rate can be estimated from the product of kerma rate and area, or it can be directly measured using a large area transmission ionization chamber (often referred to as a KAP-meter). When using P_{KA} to estimate skin dose from fluoroscopy procedures, air kerma at the PERP can be estimated by dividing the measured P_{KA} by the radiation beam area at the PERP (Section 2.B). Hence, accuracy in P_{KA} depends on the accuracy of the KAP-meter, as well as the accuracy of the estimated X-ray beam area.

Patient skin dose estimation can use the two primary dose indices of air kerma ($K_{a,r}$), located at the PERP, and the air kerma-area product (P_{KA}). The measurement of these dose indices is expertly discussed in the Report of AAPM Task Group 190.¹⁴

The air kerma at the PERP has numerous denotations in the literature ($K_{a,r}$, AK , AK_{PERP} , K_{PERP} , $K_{a,PERP}$, RAK , etc.) and will, for simplicity, be denoted K in the present report.

2.B. Patient exposure reference points for X-ray Angiography (XA) equipment

This report focuses on the single most used FGI device, a C-arm having a fixed isocenter and an image receptor that can be moved relative to the X-ray tube. Table I lists the locations of the PERP for different types of fluoroscopy device types, that is, not exclusively fixed C-arm equipment. The

TABLE I. *K* reference point locations and specifications for different fluoroscopy systems.^{1,15}

Fluoroscopic device type	Reference Point Location (IEC 2010)
C-arm	15 cm from isocenter toward the X-ray source along the beam axis or <ul style="list-style-type: none"> for C-arm equipment without an isocenter, the manufacturer defines a point along the beam axis as being representative of the point of intersection of the beam axis with the patient surface; the rationale for the choice of the location should be given. at the point representing the minimum focal spot to skin distance for C-arm equipment when the focal spot to image receptor distance is less than 45 cm.
X-ray tube under tabletop	1 cm above tabletop
X-ray tube over tabletop	30 cm above the tabletop with the end of the beam-limiting device or spacer positioned as closely as possible to the point of measurement
Fixed laterally projected fluoroscopy	Same as for C-arms 15 cm from the centerline of the X-ray tabletop and in the direction of the X-ray source with the end of the beam-limiting device or spacer positioned as closely as possible to the point of measurement. If the tabletop is movable, the tabletop shall be positioned as closely as possible to the lateral X-ray source, with the end of the beam-limiting device or spacer no closer than 15 cm to the centerline of the X-ray tabletop.

distance between X-ray source and PERP (d_{PERP}) should be confirmed from the FGI device documentation, as the manufacturer is free to use alternative locations of the reference point for specification of *K*.

The IEC provides guidance for test geometries that relate to the stated values of *K*.¹⁵ As indicated in the IEC documentation, the manufacturer reported values should include test geometries that are required to specify equipment configuration, orientation of the X-ray beam, tabletop in or out, anti-scatter grid in or out, X-ray beam entrance field size, operating settings (to be representative of normal use), technical details of parameters included in each mode of operation, frame rate, as well as selectable added filters automatically applied.

2.C. Parameters from FGI devices related to *K* and PKA in DICOM RDSR

The automatic exposure control (AEC) logic in FGI devices is designed to ensure sufficient image contrast, temporal and spatial resolution required for operators to accurately visualize small devices and anatomical structures in motion, while minimizing image noise and patient dose.¹⁶ Further information on AEC operation for FGI devices can be found in the Report of AAPM Task Group 125¹⁷ and by Gislason-Lee et al.^{18,19}

Since the AEC continuously alters exposure parameters during, and between, irradiation events in FGI procedures (i.e., continuous actuations of the device irradiation switch), the information required for calculating patient skin dose can be extensive. Fortunately, for each exposure event, parameters such as tube voltage, tube current, pulse duration, spectral filtration, and *K* can be found in the DICOM RDSR information, together with pertinent information on C-arm angulation and object distances.

Skin dose estimation based on RDSR information is restricted to post procedure calculations. Manufacturers of FGI devices have access to further (continuous) descriptions of procedural parameters to allow for estimation and presentation of skin dose in real time, which is discussed in Sections 3.B.3 and 3.B.4.

2.C.1. X-ray tube voltage and beam quality

Generally, for FGI devices, the X-ray tube voltage (kV) is programmed for an individual irradiation event to maintain an adequate X-ray beam transmission under conditions of varying patient thickness or tissue density. The RDSR provides the kV value that was used as an irradiation event average, where an irradiation event is defined as the exposure sequence resulting from a single depression of the exposure switch.

In FGI devices, spectral filters comprised of metallic sheets of aluminum (Al) and copper (Cu) are used to preferentially remove low energy photons from the X-ray beam. Figure 1 illustrates this with simulated 100 kV beams without spectral filtration, as well as with spectral filters of nominal thickness between 0.1 and 0.4 mm Cu.^{20–22} The movement of spectral filters into and out of the beam is controlled by the AEC logic.

Addition of spectral filters has a substantial effect on the beam quality. Figure 2 shows the half-value layer (HVL) of simulated 60–120 kV beams attenuated with nominal thicknesses of 0.1 and 0.4 mm/Cu, respectively.^{20–22}

The term “Flat filtration” is used in DICOM for spectral filters. Filtration is a major determining factor of the overall beam quality, and consequently also skin dose, for many FGI devices, as exemplified in Figs. 1 and 2, respectively. The RDSR specifies the minimum and maximum added flat filtration that has been used in an irradiation event.

The X-ray beam quality is typically described by the combination of kV and HVL (mm Al). These two descriptors may be used for simulation of beam quality, as used with Monte Carlo methods for determining patient dose from fluoroscopic procedures.²³ From a regulatory viewpoint, the IEC and FDA specify minimum allowable HVLs for the clinically relevant range of kV values.^{16,24}

The National Electrical Manufacturers Association (NEMA), in the NEMA Publication XR 31-2016: Standard Attributes on X-ray Equipment for Interventional Procedures, have proposed that a minimum of 0.3 mm added Cu spectral filtration should be available in FGI devices.²⁵

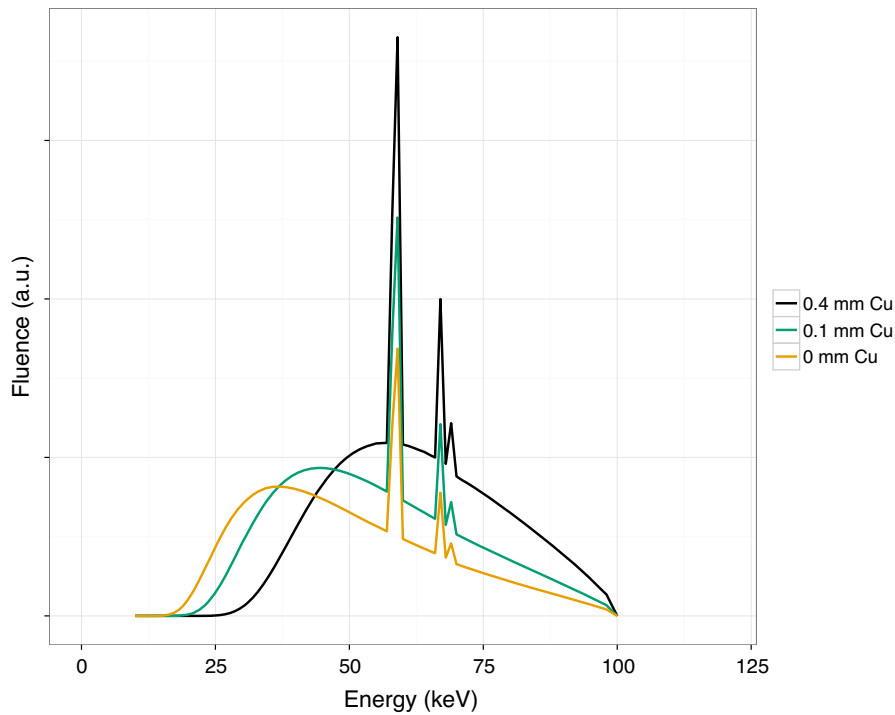


FIG. 1. The influence of Cu spectral filtration on 100 kV X-ray spectra. Simulated spectra were normalized to result in equal air kerma. Due to the decreasing mass energy-absorption coefficient of air with increasing X-ray beam energy, the “0.4 mm Cu” beam contains 25% more photons than the inherent filtration “0 mm Cu” beam.^{20–22} [Color figure can be viewed at wileyonlinelibrary.com]

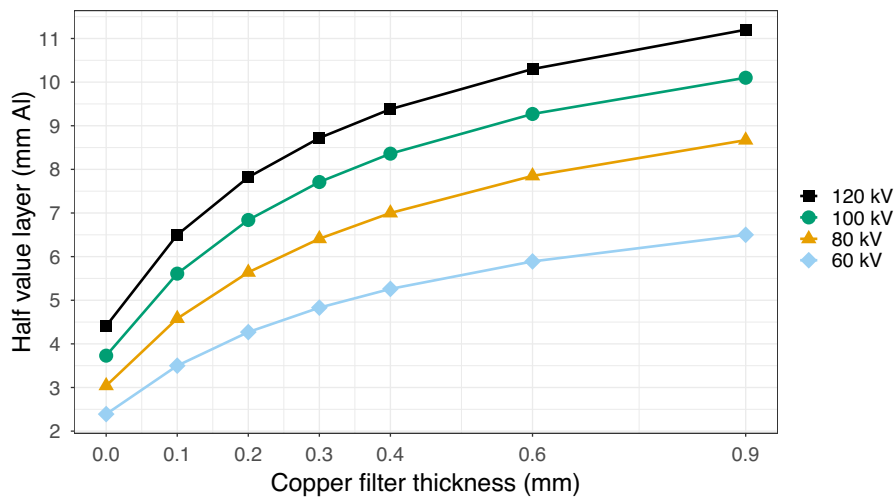


FIG. 2. Example of the influence of Cu spectral filter thickness on HVL for 60–120 kV beams.^{20–22} [Color figure can be viewed at wileyonlinelibrary.com]

2.C.2. X-ray tube current

All modern FGI devices employ a variation of high frequency generators and pulsed fluoroscopy for generating the X-ray tube current (mA), where the pulse frequency commonly varies between 0.5 and 15 pulses/s (pps) for typical clinical tasks.^{26,27} The pulse durations may also be varied and depend upon the dose rates (image quality) required for a given clinical task. The RDSR includes information of the mA per irradiation event, as an event average.

For some FGI devices, *K* is nominally proportional to the pulse rate. With such devices, reducing the fluoroscopy pulse rate from, for example, 15–7.5 pps will reduce the exposure by approximately 50%. For other devices, this relationship may be nonlinear as the system attempts to maintain uniform image quality of moving objects in the patient as the pulse rate is changed. For such devices, a “perception neutral” exposure per pulse achieves an average dose saving of approximately 50% when lowering the pulse rate from 30 to 7.5 pps.²⁸

2.C.3. X-ray beam aperture and collimation

Beam collimators in FGI devices have both primary and secondary controls. Primary collimation settings or, equivalently the selected image receptor size, affect both the X-ray beam size and magnification of the image on the display. Secondary collimation, or general “collimation”, employs leaf collimators to further reduce the size of the X-ray beam, but do not affect subject magnification. DICOM content does not currently require reporting of settings of collimation leaf shutters, nor does it document the collimation (and detector) rotation about the Source to Image Distance (SID) line through isocenter. In some cases, where information on collimation exists in the RDSR, the reported values may be restricted to square beams even if the actual field shape was rectangular.

Interventional X-ray systems include semi-transparent wedge filters, which are introduced to preferentially attenuate the primary X-ray beam. Wedge compensation filters are extensively used in cardiac and peripheral FGI procedures and block regions of low patient attenuation (i.e., lung), or cases where the FGI device imaging detector is partially directly irradiated. Details of wedge compensation filter composition and placement within the X-ray beam are not available in the DICOM content. Consequently, overestimation of local skin dose is possible.²⁹

2.C.4. DICOM information pertinent to skin dose estimation

The Report of AAPM Task Group 246 and EFOMP for patient organ dosimetry in CT includes a summary of DICOM information in the container structure of the RDSR, which is similar to fluoroscopy RDSR.³⁰

Fluoroscopy RDSR provides a cumulative total summary for a procedure and a list of irradiation event details, for both fluoroscopy and digital (stationary or rotational) acquisitions. Each time a physician depresses the fluoroscopy foot pedal during a procedure, each irradiation event with all the associated information is stored and reported in the RDSR, making applied patient dosimetry with fluoroscopy the potentially most data intensive field in diagnostic medical physics.

Thus, it is vital that medical physicists have the competence to access, read and interpret DICOM information for optimization and QA purposes. A useful exercise is to review FGI device DICOM content for their compliance with NEMA standards and manufacturer documentation. Table II contains a list of DICOM RDSR items pertinent to skin dose estimation.

There can be variations in how FGI device manufacturers populate the RDSR items shown in Table II. Furthermore, manufacturers may complement their RDSR data with further useful information. There are several good examples, for example, the distance from the central point of the collimated X-ray field area to the upper, lower, left and right field edge, in the plane located at 1 m from the X-ray source, instead of

TABLE II. DICOM RDSR items pertinent to skin dose estimation

DICOM RDSR Item	Unit	Comments
Plane Identification		Identification of acquisition plane: “Single plane” for single plane systems (one X-ray tube), “Plane A” or “Plane B” for biplane systems, taken by the posterior or the lateral X-ray tube.
Distance Source to Patient/ Distance Source to Isocenter	mm	Distance from source to center of field of view. Traditionally referred to as Source Object Distance (SOD). Typically, the distance from X-ray source to the device rotational isocenter.
Distance Source to Detector	mm	Distance from X-ray source to image detector plane. Traditionally referred to as Source Image Receptor Distance (SID).
Collimated Field Area	m ²	X-ray field area at image detector plane
Dose RP	Gy	Measured or calculation model stated PERP air kerma free-in-air
Irradiation Event Type		Identification of irradiation event type: “Fluoroscopy” for fluoroscopic event, “Stationary Acquisition” for stationary image acquisition, “Rotary Acquisition” for rotational image acquisition.
kVp	kV	Voltage applied on X-ray tube
Positioner Primary Angle	°	Position of X-ray beams incidence angle in the RAO ^a /LAO ^b direction
Positioner Secondary Angle	°	Position of X-ray beams incidence angle in the CRA ^c /CAU ^d direction
Table Height Position	mm	Height of patient support table in relation to arbitrary reference point. Positive direction may vary for different vendors.
Table Lateral Position ^e	mm	Lateral position (in CRA/CAU direction) of patient support table in relation to arbitrary reference point
Table Longitudinal Position ^e	mm	Longitudinal position (in RAO/LAO direction) of patient support table in relation to arbitrary reference point
Filter Material		X-ray filter material, either copper, or aluminum
Filter Thickness Max	mm	Maximum thickness of added filtration
Filter Thickness Min	mm	Minimum thickness of added filtration

^aRight Anterior Oblique (RAO).

^bLeft Anterior Oblique (LAO).

^cCranial (CRA).

^dCaudal (CAU).

^eThis is the definition of lateral and longitudinal directions in DICOM RDSR, which may be counterintuitive to the definition of lateral being cross-table and longitudinal being along the long axis of the table; the defined direction needs to be understood in skin dose mapping when comparing with tableside display information (also see Section 3.2).

the Collimated Field Area. For a given FGI device model, there may also be variations in RDSR content depending on the device software version. AAPM Task Group 357 and EFOMP recommend that a medical physicist should verify

FGI device RDSR information as part of commissioning, acceptance testing, and following software upgrades.

In the present review of methods for estimating patient skin dose with FGI devices and associated DICOM information, AAPM Task Group 357 and EFOMP have identified data that would be beneficial for more accurate applied dosimetry in the future. Brief descriptions are given below.

- *End Position of a fluoroscopic event.* Currently, only the start position of a fluoroscopic event is contained in the RDSR. The end position of an irradiation event would be a helpful addition.
- *Collimator Shape.* Currently, and even with the IEC 61910-1 driven extensions, the collimator is described as a rectangular shape. The DICOM Image Objects describes the collimator in detail based on the pixel data (row and column offsets). This model cannot be used in a RDSR, as there are no pixels. Referencing a certain point (e.g., Patient Reference Point or Center of Beam projected in Detector Plane or Isocenter) may help provide a solution in descriptive parameters since current beam size is defined at the intercept of the beam and the image receptor.
- *Patient Position relative to Tabletop.* The currently available DICOM patient positioning (e.g., “head first, supine”) only gives a rough outline on the patient orientation relative to the FGI device. On the other hand, an elaborate coordinate system already exists within the equipment (e.g., C-arm relative to tabletop) with arbitrarily chosen origins. A need exists to harmonize patient positioning with better granularity among manufacturer approaches. Inclusion of the patient position with a patient coordinate system with defined orientation and coordinate origin would be helpful. For example, two plausible “real-world measurable values” for recording the length from the table head to the head of the patient and that to the feet of the patient offset.
- *Field of view (FOV), Collimator.* The current “Collimated X-ray field size” and a potential future “Distances of Horizontal/Vertical Collimator Blades” may not be sufficient. Currently, the RDSR does not provide content on the collimator leaf positions on an event level basis. A future beneficial requirement may be that the detector plane FOV needs to be described within a coordinate system (referencing to a common room coordinate origin) or within a Patient Coordinate system referenced to the patient coordinate system origin.
- *Attenuation.* Methods to record (separately) the table and pad attenuation could be added to the RDSR. The values would need to be determined by X-ray beam quality and C-arm angulation, and thus, their acquisition is complicated.
- *Water Equivalent Values.* Estimates of the approximate thickness of the patient for the beam to transverse are incorporated into the AEC system with all manufacturers. It would be helpful for the user to be aware of “water values” for a given irradiation event. Such

information can be very useful in the optimization of FGI device settings.

3. CURRENT AND EMERGING METHODS TO ESTIMATE PATIENT SKIN DOSE

Since the X-ray beam may change in both intensity and position over the course of an FGI procedure, as well as over the beam area due to the heel effect, skin dose will vary from point to point. Estimation of skin dose should include dose from all sources such as the primary beam, backscatter from the patient, as well as scatter from other objects present during FGI procedures, such as the tabletop and pad. Skin dose is normally estimated on the skin entrance surface, where the beam initially strikes the patient. However, skin exit dose should also be included in certain situations, for example, small body parts, or other areas of the skin where C-arm angulation yields significant entrance and exit dose components. In general, the exit side is unlikely to contain the region of PSD unless it is also on the entrance side during parts of the procedure, for example, for rotational angiographies and Cone Beam CT (CBCT) applications in fluoroscopy.

3.A. Basic skin dose metrics

To conduct basic skin dose estimations, not taking the X-ray beam angulation and patient position into account, the relationship between K and absorbed skin dose D_{skin} must be established. Skin dose can be expressed as

$$D_{skin} = K \prod_i k_i, \quad (2)$$

where k_i corrects for the factors that differentiates D_{skin} from K .

On the left-hand side of Eq. (2), absorbed dose in matter is given by

$$D = \frac{d\bar{\epsilon}}{dm}, \quad (3)$$

where $d\bar{\epsilon}$ is the mean value of the energy that ionizing radiation imparts to matter of mass dm .³¹ In diagnostic radiology it is commonly expected that charged particle equilibrium (CPE) allows for approximating air kerma to absorbed dose, as shown in Fig. 3.³² A brief exercise on the appropriateness of employing this approximation for skin dose in FGI procedures is straightforward. The maximum X-ray beam energy that can be generated by FGI devices is approximately $h\nu = 125$ keV, and the most energetic charged particles to consider will be unbound electrons that are released in Compton interactions, which can have a maximum energy of

$$T_{max}(h\nu) = \frac{2(h\nu)^2}{2h\nu + 511\text{keV}} \Bigg|_{h\nu=125\text{keV}} \approx 40\text{keV}, \quad (4)$$

which corresponds to an electron range of approximately 0.03 mm in water according to the continuous slowing down

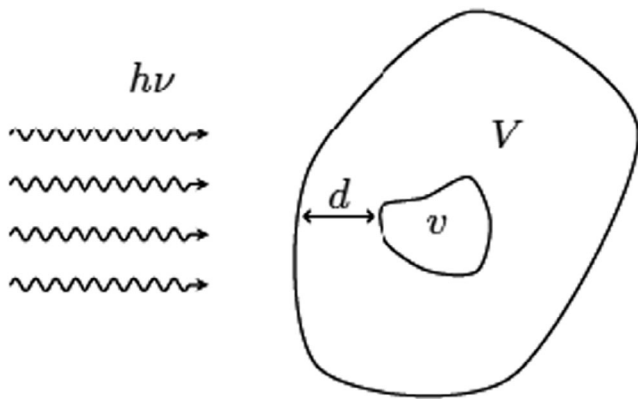


FIG. 3. Geometrical relations required for describing the CPE condition for external source irradiations, where the volume v is enclosed by volume V , with minimal separation d .

(CSDA) approximation.^{33,34} Since X-ray spectra have mean energies lower than the set FGI device kV (e.g., Fig. 1), and the thickness of human skin is much greater than 0.03 mm, it is thus reasonable to approximate $D_{skin} \approx K$.

Basic skin dose estimates can be performed for each FGI procedure irradiation event by employing correction factors for physical dependencies to K , that is, irradiation geometry, conversion of air kerma to absorbed skin dose, scattered radiation, and pre-patient attenuation (tabletop and pad). Considering these corrections, Eq. (2) can be reformulated as

$$D_{skin} = K \prod_i k_i = K k_{isq} k_{BS} k_f k_{(T+P)}. \quad (5)$$

Here, k_{isq} is the correction for source to skin distance, k_{BS} and k_f are Monte Carlo simulated corrections for back scatter and kerma in a medium different from air, respectively, $k_{(T+P)}$ corrects for tabletop and pad attenuation and forward scatter, which needs to be measured for a specific FGI device and combinations of tube voltage and filtration. A graphical description of the correction model in Eq. (5) is presented in Fig. 4. These correction factors are discussed in detail in the following sub-sections.

This basic approach of skin dose estimation avoids the complexity of modelling involving C-arm angulation, X-ray beam intensity variations and patient position on the tabletop, while sacrificing the added accuracy provided by such models. However, basic estimates of skin dose may serve as worst-case scenarios in clinical review to select patients for further investigation and follow-up of suspected skin damage.

3.A.1. The backscatter factor

The backscatter factor describes the ratio of the dose at the entrance surface of an object (phantom or patient), to the dose at the same point in air without the object, which can be measured with an ionization chamber or be determined by Monte Carlo methods. The backscatter factor for skin dose estimation represents the ratio of air kerma with backscatter from the patient body to K (i.e., without backscatter). The

amount of backscatter from the patient depends on the primary X-ray beam quality (HVL and kV), the size of the beam at the entrance surface, the thickness and material of the scattering object, and the source to skin distance (SSD). The backscatter factor typically increases with increasing HVL and kV, increasing beam size, and increasing object thickness, while displaying only a small dependence on the SSD.

Historically, the most used work for backscatter factors was provided by Petoussi-Hens et al. for ICRU soft tissues for a range of diagnostic quality X-ray beams for entrance field sizes from $10 \text{ cm}^2 \times 10 \text{ cm}^2$ to $25 \text{ cm}^2 \times 25 \text{ cm}^2$.³⁵ Figure 5 gives backscatter factors measured by Harrison for water with thermoluminescent dosimeters (TLDs) for $2 \text{ cm}^2 \times 2 \text{ cm}^2$ to $30 \text{ cm}^2 \times 30 \text{ cm}^2$ fields for HVLs from 1 to 4 mm Al.³⁶

Backscatter was shown by Petoussi-Hens et al. to be 6%–9% higher for polymethyl methacrylate (PMMA) compared to water, while backscatter for ICRU soft tissue was less than 1% larger than for water.³⁵ Thus, appropriate corrections should be applied when estimating skin dose from measurements using a PMMA phantom.

More recently, comprehensive works on backscatter factors employing Monte Carlo methods for X-ray beam qualities and field sizes representing modern fluoroscopy equipment have been done by Benmakhlouf et al.^{1,2,37,38} Beyond these works, Benmakhlouf et al. (2011b) supplied extensive tables of backscatter factors and poly-energetic mass energy-absorption coefficient ratios (see Section 3.A.2. for application).³⁹ Benmakhlouf et al.² also studied the influence of patient thickness and found that backscatter factors reach a plateau for a water equivalent thickness over 13 cm, while supplying correction factors for lesser thicknesses (e.g., for use in pediatric FGI procedures).³⁹

Factors affecting backscatter corrections: Most works provide backscatter factors along the central axis of the X-ray beam. However, for the purpose of skin dose estimation, it cannot be assumed that the backscatter field is uniform and that it drops to zero outside the beam edge.⁴⁰ For example, experiments performed by Rana et al. have shown that backscatter at the edge was 90% compared to the center of the field.⁴¹ Furthermore, the same work reported that 20% of the primary beam intensity was found just outside the edge of the beam, with a decline to 3% at a position 6 cm from the edge. X-ray beam intensity variations, due to the heel effect, field size, tube voltage and spectral filtration, are important for backscatter corrections in PSD estimation in FGI procedures with overlapping fields.^{41,42}

To illustrate the variability and dependencies of backscatter factors, Fig. 6 shows the ratio of exposure from a $6 \text{ cm}^2 \times 6 \text{ cm}^2$ X-ray beam measured with an ionization chamber on the entrance surface of a number of different phantoms, compared to that of a $30 \text{ cm}^3 \times 30 \text{ cm}^3 \times 20 \text{ cm}^3$ block of solid water.⁴¹ These phantoms included a 16-cm diameter cylindrical water-filled jug, a 16-cm CTDI phantom, a modified ANSI head phantom using PMMA and aluminum, a

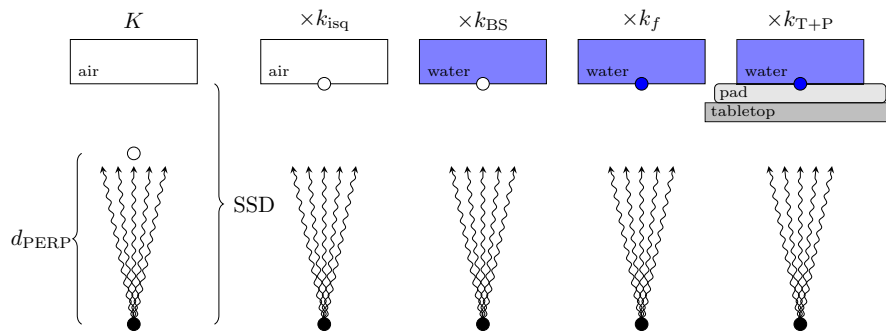


FIG. 4. Step-by-step correction of the FGI device indicated K to a skin dose estimate according to Eq. (5). The location of the measurement point is indicated with a white dot or a blue dot, respectively, depending on whether the measurement point is considered air or water equivalent.^{7,8} [Color figure can be viewed at wileyonlinelibrary.com]

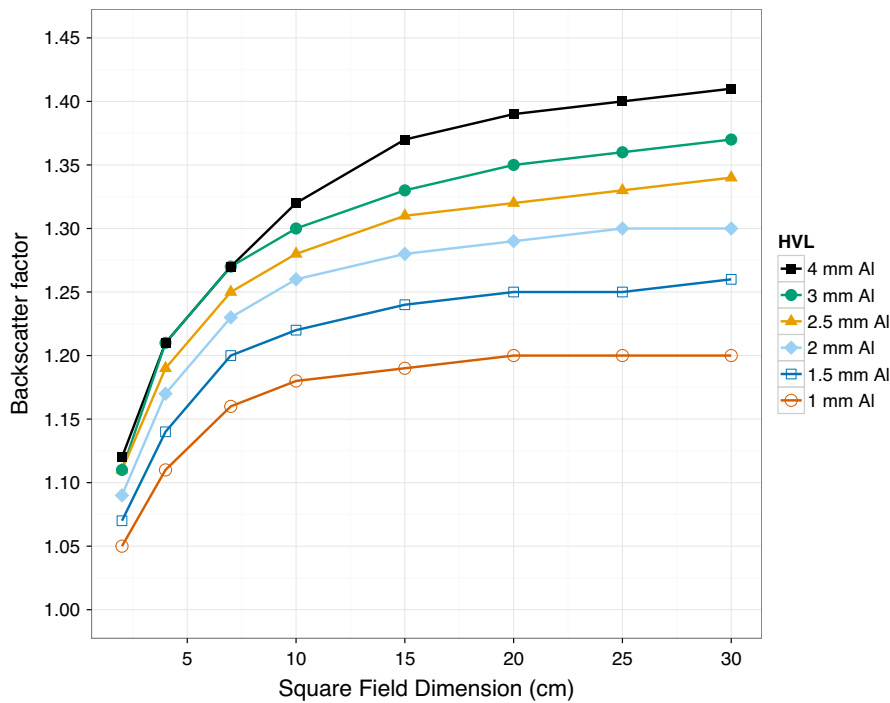


FIG. 5. Backscatter factors as a function of dimension of a square field at the entrance surface of a water phantom for different HVLs.³⁶ [Color figure can be viewed at wileyonlinelibrary.com]

30 cm³ × 30 cm³ × 20 cm³ PMMA block, as well as three head phantoms containing bone (Phantom Lab SK150, Kyoto PBU50, and Universal Medical RS240T).

Some important findings can be noted in Fig. 6. Ratios for two of the head phantoms (SK150 and RS240T) were about 5% less than the solid water phantoms, which may be due to the curvature and smaller size of these head phantoms, or due to the underlying bone near the surface, as shown by Anderson et al. and Compagnon et al., respectively.^{43,44} Ma et al. have also shown that X-ray beam size will further affect the backscatter factor values in geometries with underlying bone tissue.⁴⁵ Omar et al. (2014) investigated the influence of cranial bone on backscatter factors, where up to a 15% reduction in skin (surface) dose was found in a water phantom containing cranial bone.⁴⁶ The authors also found that further skin dose reduction can be expected with increasing thickness of

simulated bone layers, softer incident X-ray beams, and larger X-ray field sizes.⁴⁶ Furthermore, as seen in Fig. 6, the CTDI phantom ratios were lower than those for the PMMA block by about 6%, while ratios for the Water Jug were 5% less than for the solid water phantom. These results underline the importance of experiment design when estimating backscatter factors.

3.A.2. The f-factor

The f-factor is the conversion factor from exposure, or air kerma, to absorbed dose in a material of interest. Figure 7 and Table III show the f-factor variation as a function of photon energy for soft tissue, muscle, lens of the eye, cortical bone, and compact bone, calculated using the mass energy-absorption coefficients provided by NIST.⁴⁷ The f-factor for

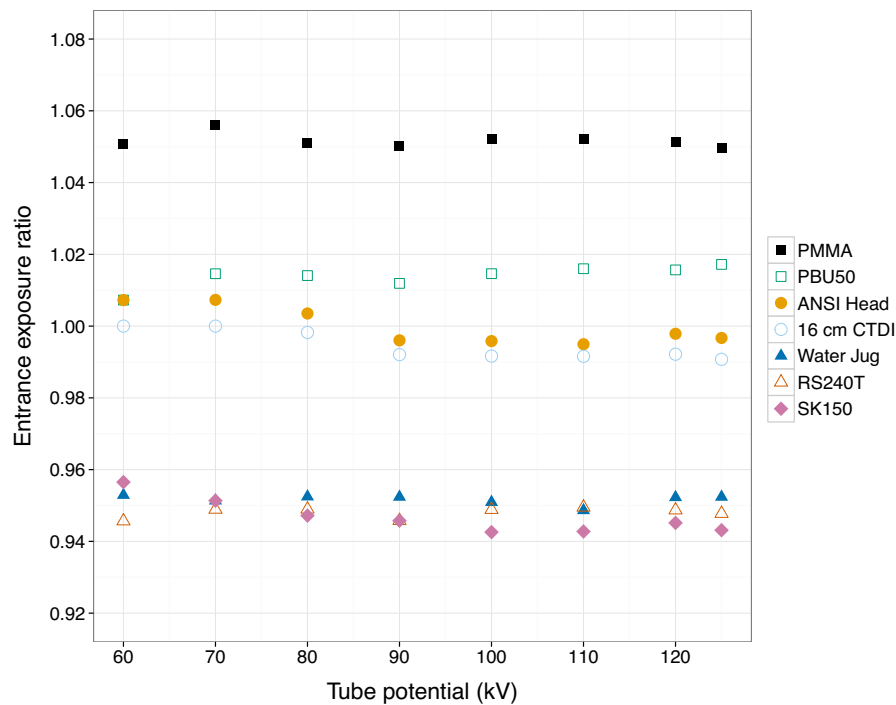


FIG. 6. Ratio of entrance exposure for various phantoms compared to that of a block of solid water as a function of kV (1.8 mm Al added filtration) for a 6 x 6 cm² X-ray beam.⁴¹ [Color figure can be viewed at wileyonlinelibrary.com]

skin is commonly considered equal to the value for soft tissue and should reflect a weighted sum by the X-ray beam energy spectrum. Seuntjens et al. have noted that the soft tissue f-factor is a function of both kV and HVL, covering a range of 1.04 to 1.07 for soft tissue.⁴⁸ The f-factor value at 40 keV of 1.06 in Fig. 7 is commonly employed for diagnostic and interventional radiology X-ray beams.

Schauer et al. showed that the f-factor depends on bone type, the extent of filtration, and beam energy.⁴⁹ Because of the larger f-factors, the dose to bone near the entrance surface can be many times higher than that of the overlying skin due to local absorption in the bone, in line with the discussion on backscatter factors in Section 3.A.1.1.

3.A.3. Distance from the X-ray beam source

The measured air kerma in a primary X-ray beam is commonly expected to decrease according to the inverse square law. Deviation from this formalism may be caused by the presence of scattered, leakage, or off-focal radiation. These factors tend to make the beam intensity reduction with distance lesser than expected. Even if the variation of air kerma with distance from the source follows the inverse square law, inaccurate determination of the distance to the skin introduces an error in skin dose estimates. Performing air kerma measurements at several points of known incremental distance and showing the results on a semi-logarithmic plot will provide an effective focal spot location, taking into account the falloff of scatter and off-focal radiation.

The RDSR contains information on distances that can be used to estimate the SSD (e.g., source to image receptor

distance, source to isocenter distance, source to tabletop distance, isocenter to tabletop distance and tabletop to object distance). However, it is common that FGI device manufacturers populate these fields differently. It should be noted that SSD estimates from the RDSR are not exact measures, since patient weight will vary the amount of compression in the pad underneath the patient.

3.A.4. Attenuation and forward scatter in tabletop and pad

The X-ray beam reaching the patient from a vertical beam with the tube placed under the patient tabletop is attenuated by objects that intercept the beam, including the tabletop, pad, arm supports, or a head holder. Skin dose estimates also need to take into account radiation scattered from objects in the beam path to the skin, that is, forward scatter.

The total effect of attenuation and forward scatter from objects in the beam path can be estimated by using a “non-perturbing” detector such as a pancake type ionization chamber. The ionization chamber should be placed at the position of the patient (or phantom) entrance surface with the tabletop and pad in their normal position during an FGI procedure. The ratio between the measurements with and without the tabletop and pad yields the correction factor for attenuation and forward scatter, where exposure parameters are kept constant. Furthermore, Vijayan et al. have proposed a way of estimating attenuation and forward scatter from the tabletop and pad using Monte Carlo methods.⁵⁰

The transmission through the tabletop and pad is energy dependent, increasing with kV and added spectral filtration,

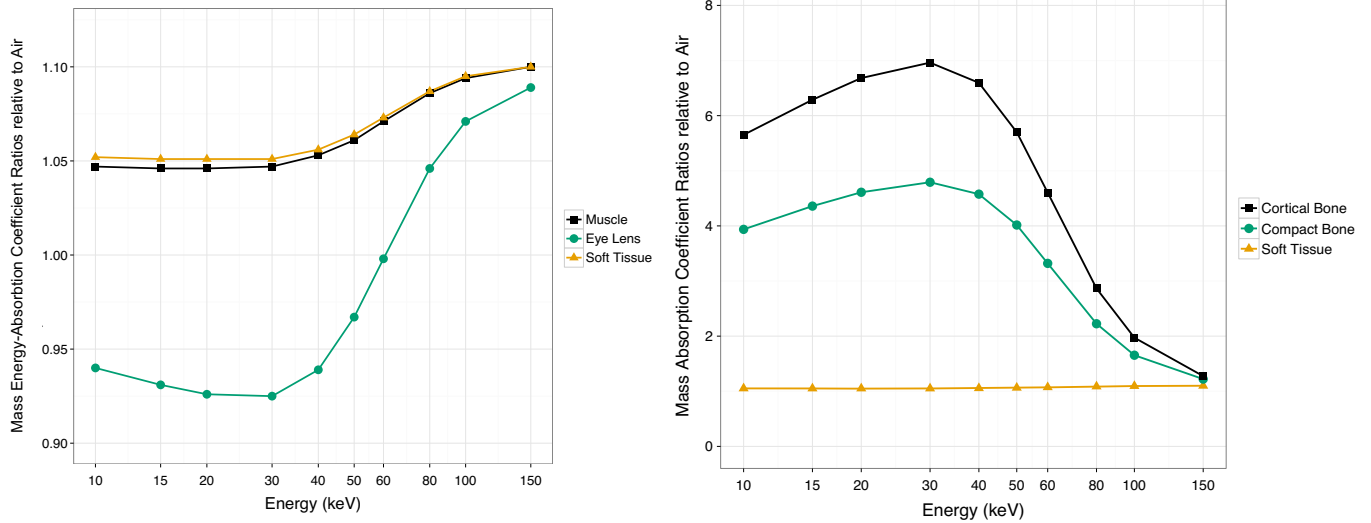


FIG. 7. Mass energy-absorption coefficients for various tissues and organs. Left: Muscle, eye lens, and soft tissue. Right: Cortical bone, compact bone, and soft tissue.⁴⁷ [Color figure can be viewed at wileyonlinelibrary.com]

TABLE III. Mass energy-absorption coefficients relative to air.⁴⁷

Energy (keV)	Soft Tissue	Muscle	Eye Lens	Cortical Bone	Compact Bone
10	1.052	1.047	0.940	5.652	3.937
15	1.051	1.046	0.931	6.288	4.359
20	1.051	1.046	0.926	6.682	4.610
30	1.051	1.047	0.925	6.962	4.792
40	1.056	1.053	0.939	6.596	4.576
50	1.064	1.061	0.967	5.700	4.016
60	1.073	1.071	0.998	4.604	3.320
80	1.087	1.086	1.046	2.865	2.225
100	1.095	1.094	1.071	1.972	1.654
150	1.100	1.100	1.089	1.275	1.221

and typically in the range of 70%–80% of the primary X-ray beam, as seen in Fig. 8. Forward scatter from the tabletop and pad is about 8%–12% of the amount transmitted so that the net effect of the tabletop and pad is a reduction of the entrance air kerma to typically 75%–85% of that without the tabletop and pad. For accuracy, measurements should be conducted to verify the extent of attenuation for the actual equipment used. Since FGI device AEC settings and anatomical protocols use a variety of kV and spectral filtration, a matrix of measurements of tabletop and pad attenuation and forward scatter factors is needed for skin dose estimation, which can be paired with RDSR information on kV and spectral filtration.^{51,52}

The transmission of the beam through the tabletop and pad is dependent on the angle of incidence and non-normal incidence requires further correction.⁵³ The path length of the central ray through a horizontal tabletop and pad is increased by the secant of the CRA/CAU (Cranial and Caudal, respectively) or RAO/LAO (Right Anterior Oblique and Left Anterior Oblique, respectively) angulation (described in

Section 3.B), and the entrance skin dose is decreased accordingly. As proposed by Rana et al., when both angles are changed, the effective path length through the tabletop and pad can be calculated as

$$t' = t [\tan^2(\alpha) + \tan^2(\beta) + 1]^{\frac{1}{2}}, \quad (6)$$

where t is the actual tabletop/pad thickness, α the angle in the RAO/LAO direction and β the angle in the CRA/CAU direction.⁴¹ In the following sections on patient models, coordinate systems and skin dose mapping, α and β denote the primary and secondary angles, respectively.

The attenuation of the tabletop (T) and pad (P) are presented as the sum of the values of, $\mu_T t_T + \mu_P t_P$ respectively, where μ is the linear attenuation coefficient and t the thickness, which can be determined by transmission measurements with normal incidence of the beam as described above. Figure 8 shows values of $\mu_T t_T + \mu_P t_P$ that were measured for the tabletop and pad on an FGI device as a function of kV for three different spectral filters.⁵⁴ Figure 8 also shows the corresponding relative transmission.

Assuming exponential attenuation, the corrected intensity at the given angulation through the tabletop and pad could be calculated using the following relation

$$I_{(\alpha,\beta)} = I_{(0,0)} \times e^{-(\mu_T t_T + \mu_P t_P) [\tan^2(\alpha) + \tan^2(\beta) + 1]^{1/2} - 1}, \quad (7)$$

where $I_{(0,0)}$ is the intensity of the beam transmitted through the tabletop with normal incidence and $I_{(\alpha,\beta)}$ is the intensity of the beam transmitted at angles α and β . This attenuation formalism and the approximation of forward scatter being proportional to the transmitted primary X-ray beam fluence have been discussed in multiple studies.^{41,51,53} Figure 8 shows an example of measured tabletop and pad attenuation and transmission,⁵¹ which may be used for PSD estimation, as discussed by DeLorezo et al.⁵¹ It should be noted that DeLorezo et al. also found that measuring and determining

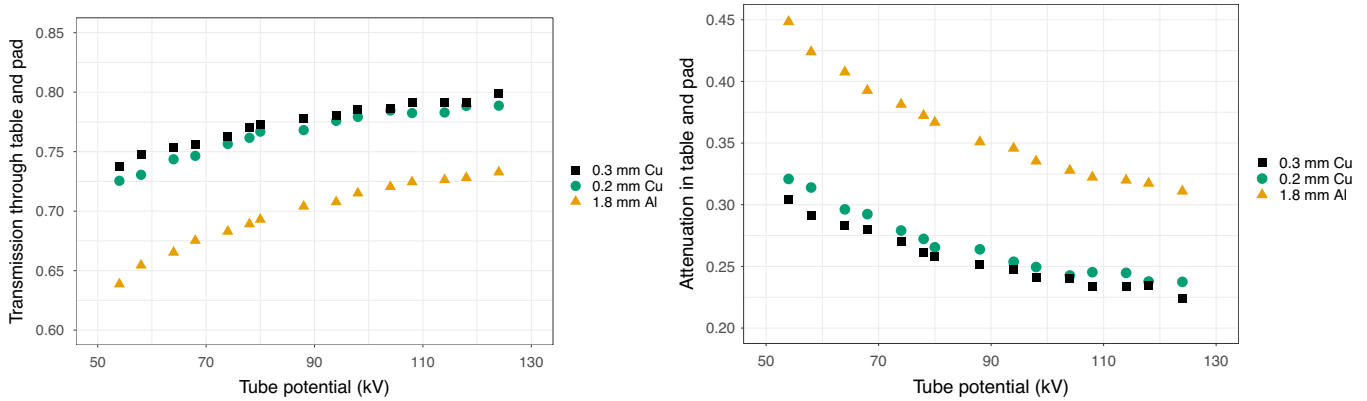


FIG. 8. Examples of measured tabletop and pad attenuation and transmission.⁵⁴ Left: the ratio of beam intensity transmitted through the tabletop and pad to the intensity measured in air, as a function of kV for the three spectral filters. Right: $\mu_{TT} + \mu_{PP}$ shown as function of kV for three different spectral filters [Color figure can be viewed at wileyonlinelibrary.com]

the total correction required due to attenuation, back- and forward scatter might improve the accuracy of these corrections.⁵¹

3.B. Refined skin dose metrics

The basic skin dose estimation formalism described in Section 3.A includes relevant physical correction factors, while omitting dependencies of X-ray beam angulations and actual patient position. A mapping tool is required to investigate and sum up multiple patient skin dose contributions during a procedure that uses C-arm angulation, that is, a more refined skin dose estimate. Mapping is needed to locate the exact region of skin that received the PSD, which also includes the need to know where a patient was positioned on the tabletop, taking physical correction factors into account. The discussion in this section is based on the open-source project PySkinDose, where readers can find Python™ scripts and a wiki describing in detail how RDSR data can be read, physical corrections made to DICOM data, as well as beam angulations and patient positions determined for estimating PSD in various mathematical phantoms.^{7,8}

A major obstacle to mapping patient skin dose is capturing the movement of the C-arm referenced to the tabletop and the relative patient position in its totality during each irradiation event. In RDSR for FGI devices, only the location of the C-arm and support system at the initiation of an irradiation event is presented. However, the FGI device itself is aware of the C-arm angulation and manufacturers may use this information for more detailed skin dose estimates. Future evolution of RDSR information should go towards a complete description of the movement of the table, considering all six degrees of freedom, that is, tilt, cradle, longitudinal and lateral panning, height, and yaw.

The angulation of the C-arm relative to the patient anatomy is indicated by the nomenclature of anatomy angle representation. C-arm movement can be patient left/right angulation, resulting in image projections that are typically labeled RAO or LAO for a supine patient. Oblique

projections are named for the side (right or left) and the body surface (anterior or posterior) closest to the image receptor. Therefore, a RAO projection has the entrance beam point (the X-ray tube) located under the tabletop on the left side of the patient and intercepts the posterior side of the patient. The other rotation moves towards the patient head or feet in a plane parallel to the long axis of the patient. This rotation results in image projections typically labeled CRA or CAU.

The DICOM standard establishes the primary (Fig. 9) and secondary (Fig. 10) angle conventions which are used in the RDSR. In combination, they serve to locate the tabletop and C-arm position relative to the patient undergoing an FGI procedure. At a “0” degree angle for both primary angle and secondary angle, the supine patient faces the image receptor (i.e., a PA X-ray projection). The positioner primary angle is defined in the transaxial plane at the isocenter with zero degrees in the direction perpendicular to the patient chest and +90° at the patient left hand side (LAO) and -90° at the patient right hand side (RAO). The valid range of primary positioner angle is $\pm 180^\circ$.⁵⁵

The secondary axis of rotation is in the patient plane and is perpendicular to the primary axis at the C-arm isocenter. The C-arm secondary angle is defined with zero degrees in the direction perpendicular to the patient chest. +90° corresponds to the cranial direction. The secondary positioner angle range is $\pm 90^\circ$.

The above discussion on DICOM geometry is reflected in the RDSR as the tabletop, patient and C-arm positions are altered. However, the tableside display values seen by the operator are patient centric (not DICOM) following the IEC standards with FGI devices. Thus, the tableside displayed values and the values obtained in the RDSR will likely differ.

3.B.1. Skin dose mapping

The total skin dose from a procedure consists of the accumulated sum of contributions from each irradiation event. Irradiation event specifics, such as beam angulation, table position, patient position and beam collimation, limit the

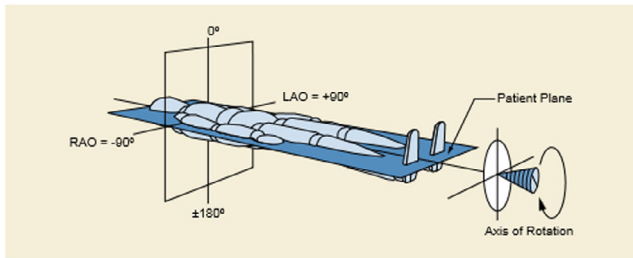


FIG. 9. A primary plane is defined as the rotation of the C-arm to the left and right, respectively.^{55,56} [Color figure can be viewed at wileyonlinelibrary.com]

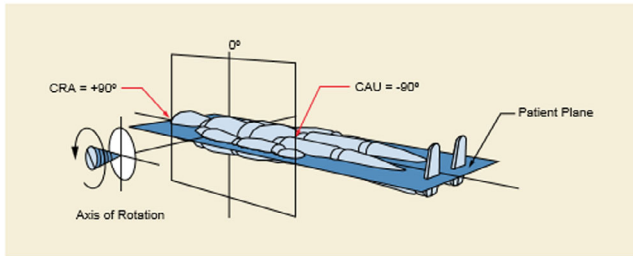


FIG. 10. The secondary angle is perpendicular to the primary angle and represents movement of the C-arm in the head and foot direction, respectively (CRA, Cranial; CAU, Caudal).^{55,56} [Color figure can be viewed at wileyonlinelibrary.com]

irradiated surface and may vary significantly between different events in a given procedure, as well as between different procedures. This results in large variation in the patient- and procedure-specific skin dose distribution. An initial approach has been to map K to a sphere, which is correlated to the PERP as visualized in Fig. 11.⁵⁷ This was done since FGI operators generally place the anatomy of interest at isocenter to facilitate visualization of, for example, a vessel centered in the image receptor. This equipment-centric approach depicts the entire exposure distribution across a sphere created by a radius of 15 cm from isocenter. The exposure incidence map is not patient skin dose, but the metric could be further improved, for example, with the physical corrections from Section 3.A. Furthermore, the incident map has limitations

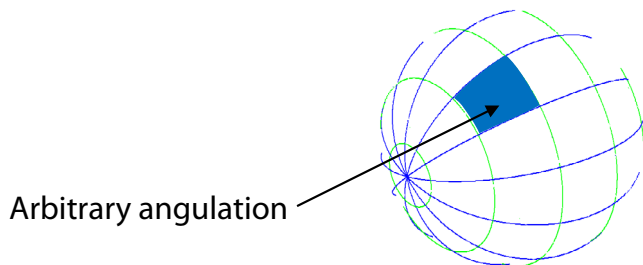


FIG. 11. If the patient's skin is located at the PERP, it is represented by the surface of a sphere with its center at the isocenter of the C-arm fluoroscopic unit. As the C-arm is angulated in every direction, projections onto the surface of the sphere define the skin dose maps for a procedure. This geometry is independent from the patient.^{57,58} [Color figure can be viewed at wileyonlinelibrary.com]

regarding the actual size and location of the patient. This spherical patient model can lead to inherent inaccuracies since it does not take into account the patient shape and location. Also, when the skin is not at the PERP, the projected X-ray field size differs from the mapping on the sphere for all distances.

A more realistic shape and location of the patient and a real skin dose calculation should overcome these limitations.⁵⁸ A common approach is to use patient-specific phantoms together with the spatial variations of accumulated skin dose to conduct a 3D skin dose mapping. In this context, a phantom describes the skin surface of the patient by a discrete number of skin patches (e.g., rectangular or triangular), each defined by its spatial coordinates. In this patient-centric approach the cumulative dose is provided for each skin patch of a virtual patient skin. Additionally, the occurrence of potential overlap of irradiated regions of skin is respected.

Patient models and computational phantoms: Several different types of computational phantoms can be used for skin dose mapping. Common stylized computational phantom types (3D rendered) are mathematical representations of spherical (as discussed above), cylindrical, or humanoid phantoms. Cylindrical phantoms are used to minimize spatial generalization errors of the acquired skin dose distribution for different patients and procedures due to problems with alignment of humanoid phantoms and the actual patient. However, Khodadadegan et al. have shown that the size of the cylindrical phantom affects the PSD estimation accuracy for increasing primary angulation.²⁹ Patient-specific 3D modelled phantoms are required in order to accurately describe the skin dose distribution for individual patients. Each phantom skin patch should optimally be accompanied by a normal vector defining the outward direction from the patient. This is required to accurately present the phantom visually and to distinguish between entrance and exit skin patches in skin dose calculations. Examples of phantoms are given in Fig. 12. More information on computational phantoms can be found in the Report of AAPM Task Group 246 and EFOMP for patient organ dosimetry in CT.³⁰

PySkinDose⁸ matches the patient to a graphic by choosing from a library of male and female 3D patient graphics with different heights and weights, which are created with the MakeHuman[®] software.⁵⁹ Figure 13 shows examples of a male graphic with two different heights and weights from a commercially available skin dose estimation system. Software solutions such as Blender[®] can be used to restructure the graphic exported from MakeHuman[®] and match the pose of the patient.⁶⁰ This is useful to raise the arms of the patient, that is, so the arms do not intercept the beam.

Geometry modelling: A description of the geometrical relation between the phantom and X-ray beam is required to perform skin dose mapping. RDSR specified parameters on beam position and collimation provide means for calculating the position of the X-ray beam for each irradiation event.

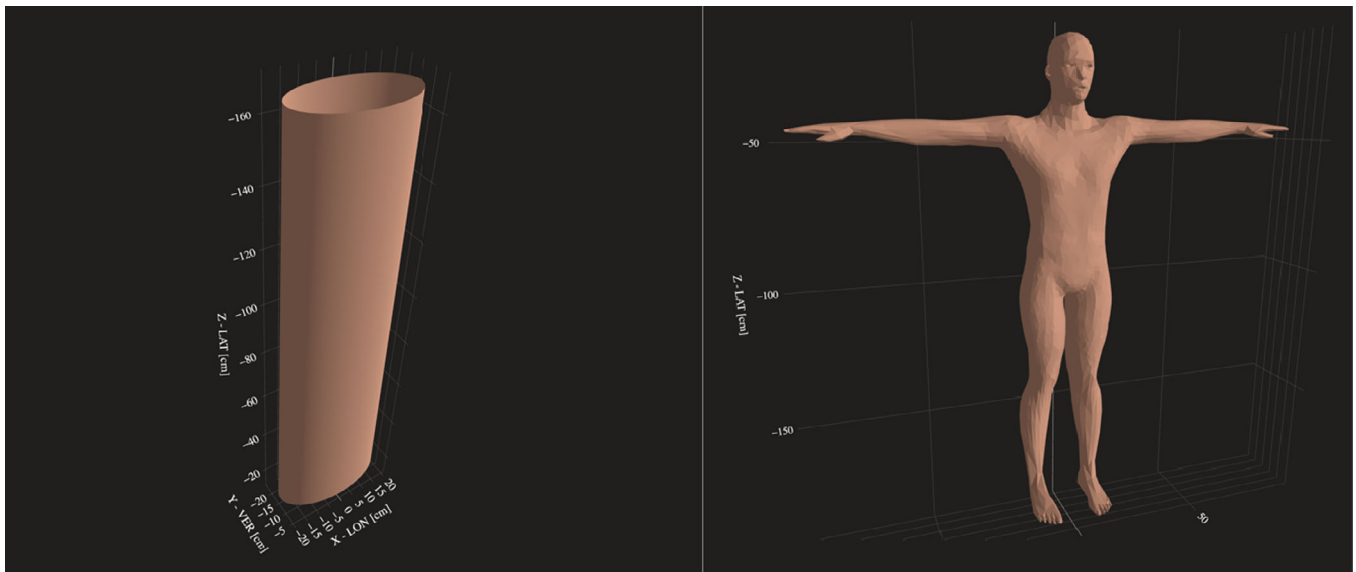


FIG. 12. Example of patient phantoms for skin dose mapping. Left: A cylindrical phantom with elliptic cross-section. Right: A human-shaped phantom, constructed with the MakeHuman[®] software.⁵⁹ Both phantoms are available in PySkinDose.⁸ [Color figure can be viewed at wileyonlinelibrary.com]

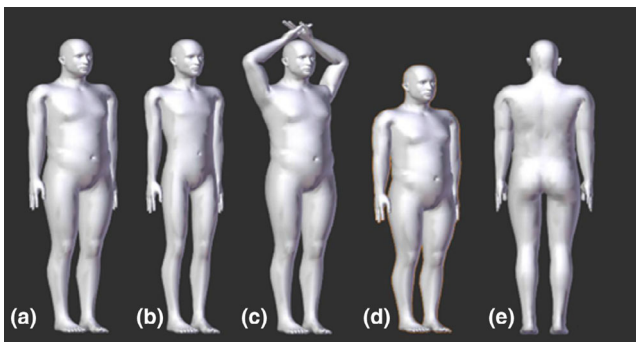


FIG. 13. Basic patient graphic displays for commercial real-time dose mapping. Note the arm position for phantom (c).^{41,59,60} [Color figure can be viewed at wileyonlinelibrary.com]

Furthermore, RDSR content also specifies patient tabletop position, upon which a phantom can be positioned.

In the RDSR structure, the position of the X-ray field is defined by the combination of the beam angulation in RAO/LAO and CRA/CAU direction, together with the beam collimation and the source to image receptor distance. The support table is defined by its displacement in the lateral, longitudinal, and vertical direction, in relation to an arbitrary reference point defined by the FGI device manufacturer. Note that the location of the X-ray beam and tabletop is stated in the RDSR with different reference points and directions. The relative position between these objects is not specified explicitly. This needs to be addressed before skin dose mapping can be performed.

A common approach is to define these objects in separate coordinate systems, followed by a coordinate transform to a common coordinate space in which the skin dose mapping can be conducted. This is illustrated in Fig. 14. With this approach, the X-ray beam is defined in a Cartesian coordinate

system, fixed to the position of the X-ray source (red in Fig. 14), while the tabletop is positioned in another Cartesian coordinate system, fixed in relation to the table (green in Fig. 14), upon which the phantom can be positioned.

For each irradiation event, the X-ray beam and tabletop can be positioned in the isocenter coordinate system (blue in Fig. 14) by deriving the displacement and rotation of these coordinate systems in relation to the isocenter. In the standard case, this mapping is a function of beam angulation and tabletop displacement. The spatial displacement is illustrated by the vectors \mathbf{r}_s and \mathbf{r}_t in Fig. 14. The point P , located by the vector \mathbf{r}_p , denotes an arbitrary point in the isocenter coordinate system, which is used to denote the dose map skin patch positions for a computational phantom on the tabletop.

Calculating the X-ray beam to patient intercept: Once the X-ray beam and phantom have been positioned in the same coordinate system, as described in Section 3.B.1.2, the next step is to calculate which patches of skin are hit by the X-ray beam. This is done to select the irradiated area for skin dose calculation.

The X-ray beam to patient intercept determination can be conducted by a variety of different algorithms. A straightforward approach is to implement an algorithm that calculates the signed distance from each skin patch, to all of the four planes that build up the extent of the pyramid shaped X-ray beam. This concept is illustrated by red fields in Fig. 15. Here, we see that the vector $(\mathbf{r}_p - \mathbf{r}_s)$ points out the position of the skin patch relative to the X-ray source, and that the skin patch is hit by the X-ray beam if the signed distance from the skin patch to all of the four planes of the X-ray beam is negative (since the normal vector \mathbf{n}_1 to \mathbf{n}_4 is directed outwards). This can be calculated by using the following algorithm, for each skin patch:

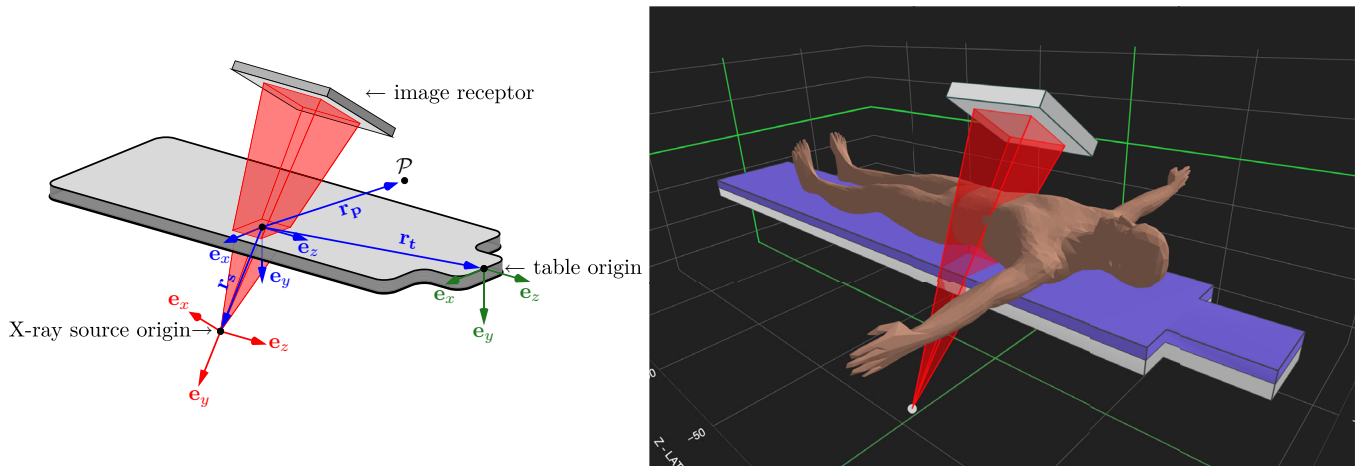


FIG. 14. Left: Illustration of three Cartesian coordinate systems, with origin fixed at the X-ray source (red), the tabletop (green), and the isocenter of the C-arm (blue). The red coordinate system is used to define the location of the X-ray beam from beam-related parameters in the RDSR structure, while the green coordinate system is used to define the position of the patient support table, upon which the user-defined patient phantom is positioned. Right: Illustration of the same geometry, when conducting skin dose mapping with PySkinDose, where the patient and the X-ray beam have been defined in separate coordinate systems and transformed to a common space which enables skin dose mapping.⁸ The position and orientation of the patient phantom, in relation to the tabletop, needs to be specified by the user. [Color figure can be viewed at wileyonlinelibrary.com]

- For $i = 1$ to 4
 - a Calculate the signed distance from the skin patch to the i -th plane: $n_i \cdot (r_p - r_s)$
- If $n_i \cdot (r_p - r_s) < 0 \forall i$
 - a Skin patch is hit
- Else
 - a Skin patch is missed

Calculating the X-ray beam to table intercept: A further important factor for skin dose mapping is the ability to determine if the X-ray beam passes through the tabletop and pad prior to when it hits a patch of skin. This information is needed in order to apply tabletop and pad correction factors on a skin patch level for each irradiation event. Figure 16 illustrates three different possible scenarios; (Left) where tabletop and pad corrections are needed for all irradiated patches of skin, (Middle) where no irradiated skin patches need tabletop and pad corrections, and (Right) a hybrid case when parts of the X-ray beam pass through the tabletop and pad.⁸

This can be achieved by implementing a Ray-Triangle interception algorithm as illustrated in Fig. 17.⁶¹ The algorithm calculates the intersection point I of a line from P_1 to P_2 with a triangle with vertices at $V_0, V_1,$ and V_2 . The algorithm parametrizes $w = s \cdot u + t \cdot v$ and returns closed form expressions for s and t . A ray passes through the triangle if $0 \leq s, t$ and $s + t < 1$, and misses otherwise.

This concept can be applied to determine if the skin dose calculation needs tabletop and pad attenuation correction for

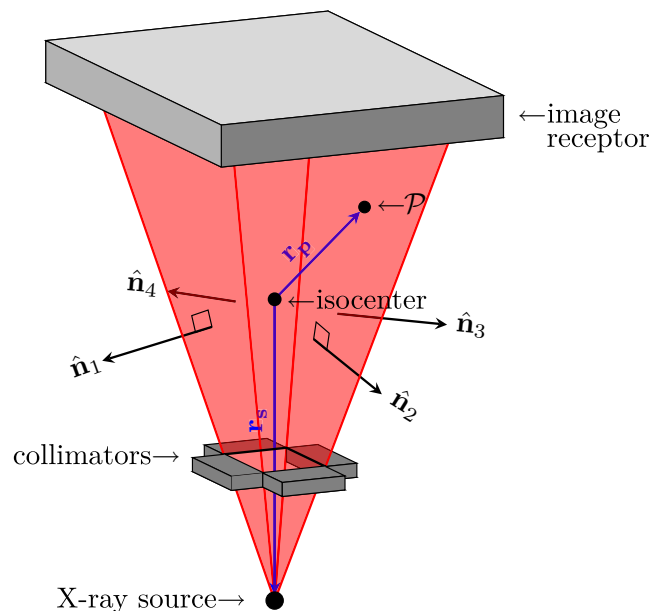


FIG. 15. Illustration of the X-ray beam-patient intercept algorithm.⁸ The algorithm calculates the signed distance from the skin patch to all of the four sides that delineate the X-ray beam. [Color figure can be viewed at wileyonlinelibrary.com]

each patch of skin. By covering the tabletop with two adjacent triangles that together span the entire surface of the tabletop, we can conclude that the single X-ray passes through the tabletop if any of the two triangles are passed (In this case, P_1 corresponds to the X-ray source, and P_2 corresponds to the skin patch). The right part of Fig. 17 illustrates how the vector w can be calculated in relation to the X-ray source and isocenter. From Fig. 17, $a + w = k \cdot r$, where k is a constant, and r is a unit vector from the X-ray source in the direction of the skin patch. Further, k can be found by

projecting \mathbf{a} and \mathbf{r} upon \mathbf{n} , which results in $k = \text{proj}_{\mathbf{n}}\mathbf{a} / \text{proj}_{\mathbf{n}}\mathbf{v}$. Solving these equations yields

$$\mathbf{w} = \frac{\mathbf{a} \cdot \mathbf{n}}{\mathbf{v} \cdot \mathbf{n}} \cdot \mathbf{r} - \mathbf{a}, \quad (8)$$

which can be provided to the Ray-Triangle algorithm together with the coordinates of the tabletop corners.

Calculating the skin dose map: A complete skin dose mapping procedure can be summarized in the following algorithm, for each irradiation event:

- Position X-ray beam, tabletop, and pad from RDSR data
- Position phantom upon tabletop and pad with procedure-specific position and orientation
- For each patient patch of skin:
 - a Check if skin patch is irradiated by X-ray beam (Section 3.B.1.3)
 - b If skin patch is irradiated:
 - Calculate if tabletop and pad correction is required (Section 3.B.1.4)
 - Calculate correction factors (Section 3.A)
 - Apply skin dose calculation to skin patch
 - Add result to skin dose map

Once the above algorithm has been computed, the skin dose distribution can be visualized as a 3D dose map. This is illustrated in Fig. 18.⁸ From this, the PSD equals the maximum absorbed skin dose to any of the patches of skin on the patient phantom.

PSD graphic element resolution: Figure 19 shows the standard native resolution of skin dose on a patient graphic obtained from the CAESAR Project library,⁶² which has been used for a prototype commercial skin dose estimation software.⁵³ Figure 19 shows the result of subdividing the triangular elements representing the irradiated area by a factor of 16.⁴¹ Agreement is much better in the X-ray beam outline

shown by the red dashed lines and the color-coded elements representing the irradiated area after subdividing the skin elements. The native resolution for this model type varies by location since the elements are formed by tessellation, which varies the element size to the surface curvature in an inverse manner (greater curvature, smaller size of elements). Subdividing elements further does not improve the curvature representation, but it does improve the ability to define the intersection of the beam edge with the patient. The improved resolution graphic shown in Fig. 19 shows 2400 elements in an $8 \times 8 \text{ cm}^2$ skin entrance field, providing elements with less than a 2.0-mm dimension between vertices of the mesh elements.⁶³ The software calculates the dose to the common vertices of these elements and significantly reduces the number of needed calculations, although several hundred were used in this field size.

3.B.2. Patient position on the tabletop

Any method for skin dose mapping needs geometry information to determine the intersection points of the X-ray beam with the patient. This requires accurate modeling of the imaging system, tabletop, and patient. A precise location of the patient position relative to the beam is also needed. Currently, the operator matches the graphical representation of a patient to the actual position of the patient on the tabletop for all commercial systems, that is, manual selection and positioning. Since skin dose varies with the patient contour according to inverse square dependence, the graphical model may need to be closely matched to the shape of the patient.

Operators can precisely match the patient location on the tabletop with the graphical representation of a patient using the following steps: (a) measure the distance of the patient from reference points on the tabletop such as the axial centerline or the head end, (b) note the patient position (e.g., supine), (c) choose a phantom with same gender and similar size and contour, and (d) match the location of the graphical representation of a patient to those distances. For this approach to be accurate:

- The graphical phantom must closely match the patient in size and body type, especially if the interventional

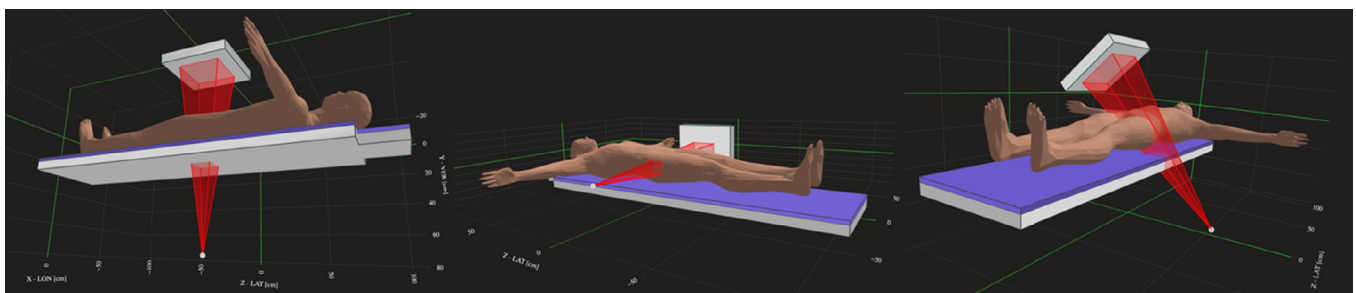


FIG. 16. Illustration of the importance of applying the tabletop and pad correction factors on a skin patch level. Left: Normal incidence posterior projection, in which all irradiated skin patches should be corrected for tabletop and pad attenuation. Middle: LAO projection, where no patches of skin should be corrected for tabletop and pad attenuation. Right: RAO projection, where parts of the X-ray beam are covered by the tabletop and pad.⁸ [Color figure can be viewed at wileyonlinelibrary.com]

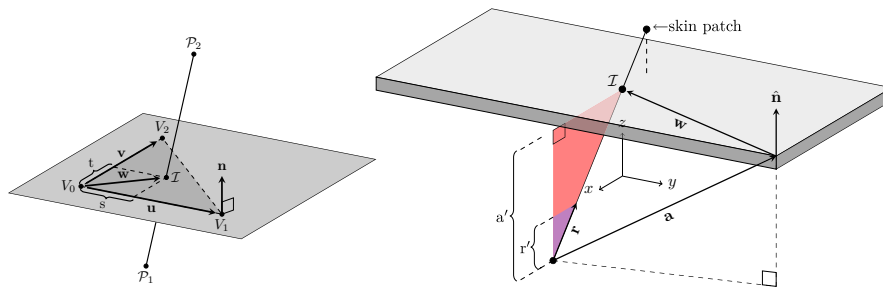


FIG. 17. Left: Illustration of the X-ray beam triangle interception algorithm where a ray from P_1 to P_2 intercepts a triangle at the point I .⁶¹ The algorithm utilizes barycentric coordinate computation, and the vector w is parameterized as $w = s \cdot u + t \cdot v$. Right: The geometrical relations between the X-ray source, isocenter, and patient skin patch required to apply this algorithm to check if tabletop and pad correction is required. [Color figure can be viewed at wileyonlinelibrary.com]

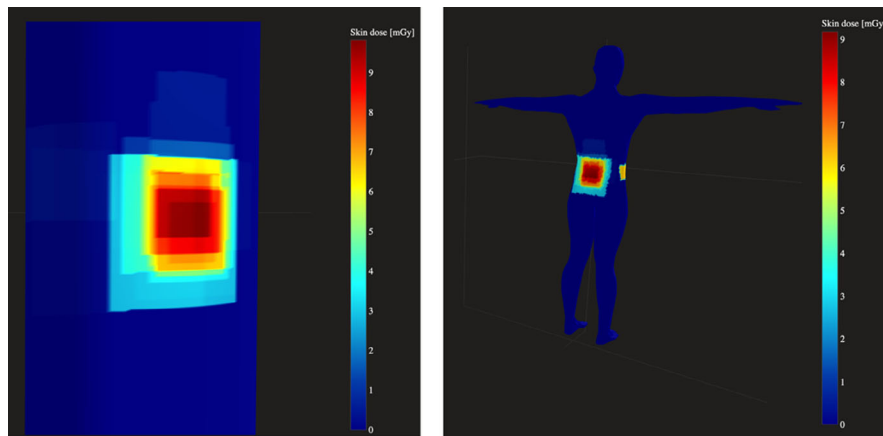


FIG. 18. Illustration of dose maps calculated from RDSR data Left: Calculated with a cylindrical phantom and Right: A human-shaped phantom.⁸ The PSD estimate equals maximum absorbed skin dose to any of the skin patches on the patient phantom. [Color figure can be viewed at wileyonlinelibrary.com]

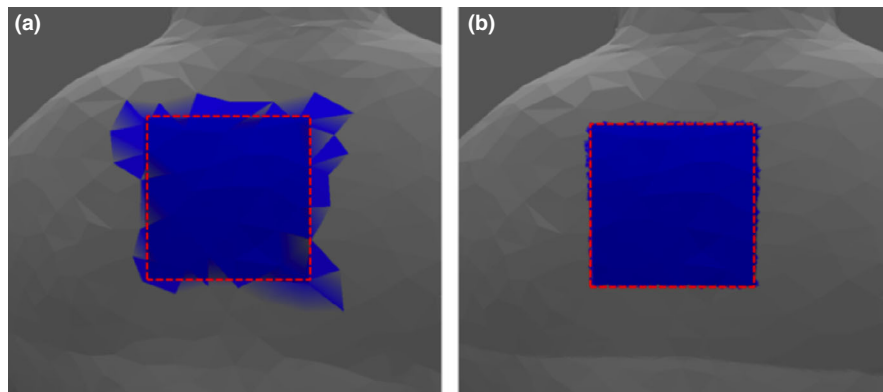


FIG. 19. (a) Skin dose pattern in blue indicated on the phantom, as represented at the native resolution of the CAESAR Project human graphic and with the actual X-ray beam outlined by the red dashed line. (b) Skin dose pattern obtained after subdividing each native graphic element into 16 elements, showing improved correspondence with the X-ray beam outline.^{41,62,63} [Color figure can be viewed at wileyonlinelibrary.com]

location is distant from the reference location. For example, using the top of the patient head as the reference might not give a good indication of beam location for a cardiac or abdominal intervention. Instead, the operator should consider choosing a different anatomic part (e.g., tip of sternum) near the target organ.

- Highly specific procedural interventions, that is, routine diagnostic cardiac catheterization, require a

location within the graphical phantom (heart) that can be automatically specified. The matched phantom coupled with C-arm angulations establishes the skin location.

- A user selectable marking (fiducial point) on an image (with fixed C-arm geometry) such as the tip of the nose, may be useful for neurological interventional procedures.

- Operators can also match the phantom to the internal structural anatomy visualized in images. The use of hybrid phantoms that include internal structure in addition to surface contour would be more suited to this approach for real time matching and skin dose determination than a simple body model graphic.

3.B.3. Real-time dose mapping

Mapping a dose distribution onto a phantom uses available data from DICOM RDSR, or, in the case of real time skin dose representations, more immediately from an FGI device component communication network. With commercial offerings, the equipment manufacturer conveys real time skin dose updates, interprets the data from the imaging system and provides an interface to computational tools.

Skin dose rates during acquisition series can easily exceed 2 Gy/min, so that very large skin dose contributions could be unknowingly reached if the updated dose rate is not displayed quickly. At a dose rate of 2 Gy/min, a 1-s *delay* sets the display behind by 17 mGy.

3.B.4. FGI device manufacturer skin dose estimation software solutions

Exposure mapping of a patient having received an FGI procedure was first performed in 2001.⁵⁷ In that case K was distributed on a sphere with 15-cm radius with a midpoint located at the isocenter. Multiple exposure or dose (i.e., air kerma or skin dose) mapping systems are now available to compute and display the distributions on the patient skin in real-time or post-procedure for use in QA and patient care. These systems implement mathematical representations of exposure by using information from dose indicators, including cumulative K and other FGI device exposure parameter settings and geometry data. The commercial applications feature calculations based on calibration files (predetermined or calibrated for each individual FGI device) or the device K . The main difference between skin dose estimation, as described in this report, to skin dose estimation with commercial software from FGI device manufacturers is the availability of exposure and geometry data. Instead of restricting the exposure data source to DICOM RDSR and image header tags, the manufacturer can access information from the FGI device continuously during every irradiation event. Hence an increased accuracy may be provided for skin dose estimation and data can be displayed in real-time to the operator (e.g., intra-event exposure parameter variations, collimation and influence of wedge compensation filters).⁶⁴

Regarding exposure or dose distribution mapping, there are three main types of solutions available:

- Skin dose mapping based on computational phantoms that are similar to the individual patient based on patient height and weight, available CT scans or operator chosen phantoms.
- Skin dose mapping based on phantoms of cylindrical- or super-elliptical shape based on BMI-matching to patient length and weight.
- Air kerma mapping on “2D-maps” based on models dividing the human body into body zones with further sub-division into body areas.

FGI operators might benefit from having a displayed value of a cumulative FOV skin dose shown in comparison to the PSD, which is an identified position mapped to the patient. Figure 20 shows an example from a commercial skin dose estimation system, where the maximum skin dose is indicated as the procedure PSD.⁶⁵ The FOV PSD value relates to the current incidence of the X-ray beam. This example shows that real time skin dose estimation may be helpful as operator movements of the beam can prevent overlap and avoid high PSD values.⁶⁵

A biplane FGI procedure requires visualization of the combined dose from both X-ray tubes. Figure 21 provides a display that shows two views of the patient undergoing such a procedure.⁴¹ Here, a single graphic patient model is used to accumulate dose from both projections so the cumulative dose can be mapped, but it also shows two views so that the effect of each tube can be appreciated individually. Likewise, separate displays are provided for the frontal and lateral tubes for the FOV PSD and dose rate, since each has its own FOV and dose rate.

Available skin dose mapping systems from FGI device manufacturers are often based on proprietary information, but descriptions of the following variables can be considered as a minimum for commissioning and validation performed by medical physicists:

- Computational phantom(s), including the identification of the specifically matched patient data or tabled value of phantom
- Method used to locate the computational phantom on the patient support system
- Assumed or corrected heterogeneity of the patient (bone, soft tissue, air, metal, etc.)
- Each radiation event of the C-arm, angulation and beam used (including agreement of match for beam size, shape, quality, attenuation of the patient tabletop and pad, etc.)
- Correction for the beam area non-uniformity (heel effect, wedge filters)
- Correction for the start, stop, and intermediate locations of fluoroscopic and acquisition events
- Uncertainty of skin dose estimates, with specifications of the criteria under which the uncertainty has been validated, which may be a standard phantom.

4. SOURCES OF UNCERTAINTY IN ESTIMATING PATIENT SKIN DOSE

For skin dose estimates from FGI procedures to yield robust and actionable information within healthcare the

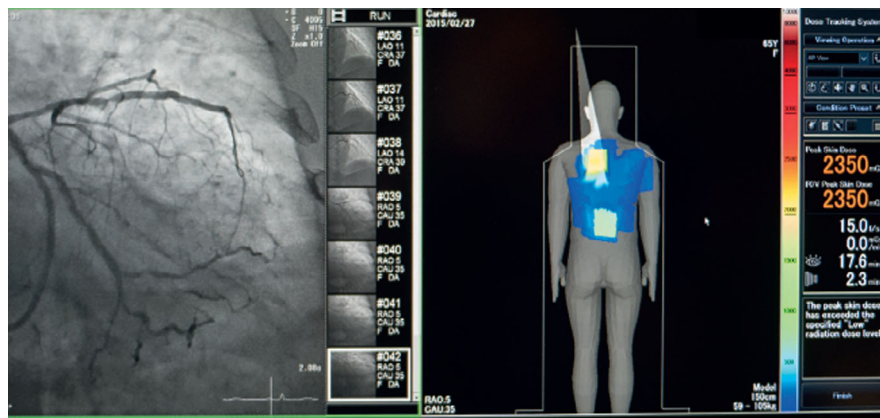


FIG. 20. Real-time skin dose distribution obtained during a cardiac PCI procedure with commercial skin dose estimation system.⁶⁵ [Color figure can be viewed at wileyonlinelibrary.com]

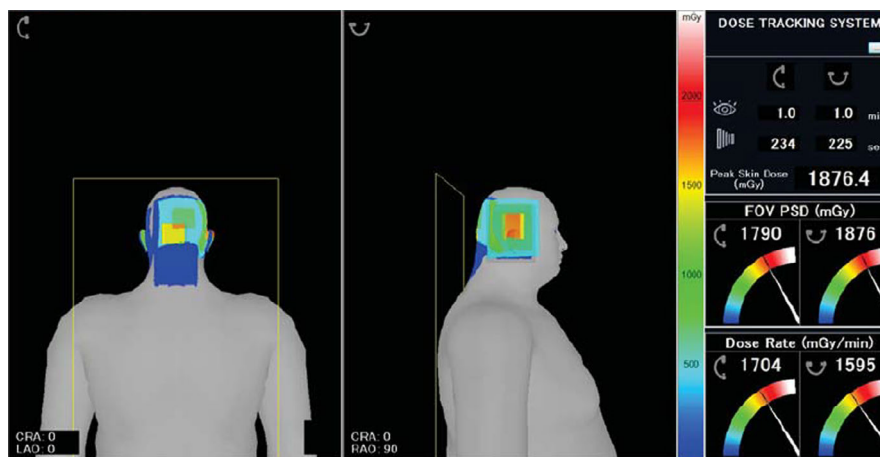


FIG. 21. Biplane dose mapping display for a simulated neuro-interventional procedure. Graphics of the FOV PSD and dose rate for frontal and lateral beams are provided in the window on the right.⁴¹ [Color figure can be viewed at wileyonlinelibrary.com]

associated uncertainties must also be known and understood. There is presently no comprehensive discussion in the literature regarding uncertainties in patient skin dose estimates, nor do commercially available software solutions communicate uncertainty with skin dose estimates. A reasonable goal would be to express skin dose and PSD estimates as expected mean values with two standard deviations (a 95% confidence interval).⁶⁶

4.A. Uncertainties associated with basic skin dose estimates

Table IV summarizes the current knowledge of uncertainties associated with basic skin dose estimates, as discussed in this report.

4.A.1. Air Kerma at the PERP

Reduction of uncertainty with skin dose estimates can be accomplished simply by performing an independent

measure of *K*, as the allowed manufacturer tolerance is ±35%.^{15,24} Medical physicists performing measurements of *K* may reduce this uncertainty to ±5%, providing a 95% confidence interval. Such measurements are helpful even when simply using the air kerma as a quality metric for patient skin dose.⁶⁷ Measurements of *K* should be performed in both fluoroscopy and acquisition modes to accommodate for different X-ray pulse generation and shape.⁴¹ A detailed description of the experimental protocols for the different types of dosimeters and their uncertainties is given in the Report of AAPM Task Group 190.¹⁴

4.A.2. X-ray beam size (Area) at the PERP

Ignoring the secondary collimation in determination of X-ray beam size may result in unfounded concern for overlapping regions of skin. Using only primary collimation, the beam size can be determined on the skin of the patient to within ±5%.

TABLE IV. Identified uncertainties associated with basic skin dose estimates, employing only physical corrections, from FGI device procedures

Source	Description	Magnitude of Error
Air kerma (K) at the PERP	a. Measurement performed by a medical physicist. b. Required tolerances by IEC and FDA. ^{15,24}	a. $\pm 5\%$, inclusive of ± 2 standard deviations. b. Up to $\pm 35\%$, stated tolerances provided by the manufacturers. ^{15,24}
X-ray Beam Size (Area) at the PERP	Correction for beam size. See the Report of AAPM Task Group 190. ¹⁴	An error with the beam size affects P_{KA} , which propagates to K for FGI devices with KAP-meters. An area that is wrongly stated as too large can cause overlapped irradiated areas when performing skin dose mapping (Section 4.2).
Tabletop and Pad Attenuation	Attenuation of primary beam by the tabletop and pad, which depends upon kV, added filtration, as well as angle of beam incidence on the tabletop.	25% to 45%.
Forward Scatter from Tabletop and Pad	Forward scattered X rays from the tabletop and pad.	8% to 12% of the primary beam.
Backscattered X rays for Soft tissue	X rays that are backscattered to the skin of the patient.	5% to 50%, depending on field size and beam quality. Up to 15% for cortical bone directly beneath the skin.
Backscattered X rays for Phantoms	Differences noted with back scatter corrections obtained using different phantom materials.	Up to 10%, depending on the actual phantom material.
Distance Correction to Skin Surface – Actual Patient versus Computational Model	Inverse square law from the X-ray source to patient. Large patients and lateral projections may be expected to cause the largest variations.	$\pm 20\%$, depending on the relative position of X-ray source and irradiated patient skin area.
Conversion of Skin Exposure to Skin Dose	Conversion of air kerma to absorbed skin dose.	Up to 4%, depending on X-ray beam energy.
Non-uniformity of the X-ray Beam	Correction for non-uniform irradiation of the patient skin, for example, from the heel effect and use of wedge compensation filters.	Up to 15%, depending on incident beam area on patient skin.

Khodadadegan et al. investigated the accuracy of X-ray beam size at the PERP with two different methods.²⁹ The X-ray beam shape was rectangular, and no secondary collimation was used. Neither method demonstrated more than 5% difference from the values reported by the FGI device. More work should be done to investigate how skin dose estimation

uncertainties are affected by secondary collimation when FGI devices calculate K from KAP-meter measurements.

4.A.3. Attenuation and forward scatter in tabletop and pad

Determination of the tabletop and pad attenuation substantially affects skin dose estimates, as discussed in Section 3.A.4. For accuracy, just like K , measurements of attenuation and forward scatter in tabletop and pad should be performed for individual FGI devices. Measurements should include non-normally incident X-ray beams for corrections to include all clinically relevant C-arm angulations. It may be expected that the uncertainty for tabletop and pad attenuation, together with forward scatter, correction ranges between $\pm 5\%$ and 10%.

4.A.4. Backscatter factors for patients and phantoms

Simulated backscatter factors have a low uncertainty in simple geometries if an appropriate phantom is used, as previously discussed. However, there is presently a gap in the knowledge on the combined effect of X-ray beam quality uncertainties and beam hardening from attenuation in tabletop and pad(s). This means that the X-ray beam quality at the skin surface is uncertain, which propagates to backscatter factors. It may be expected that corrections for backscatter with present knowledge introduces an estimated $\pm 10\%$ to 15% uncertainty in skin dose estimates.

The backscatter factor for skin regions with bone is lower than that for regions without bone close to the skin surface. More work is needed to better understand the dose to skin and bone with FGI procedures, particularly in neuroradiology.

4.A.5. Distance correction to skin surface – actual patient versus computational model

Unlike with Computed Tomography (CT), which “zeros” the tabletop position and patient anatomy with gantry lasers, fluoroscopy has no direct method of mapping a patient to the tabletop. A similar feature with FGI devices would be to map an anatomical location (tip of the nose, sternal notch, etc.) on a fluoroscopy frame for enhanced patient-tabletop referencing.

Corrections of the skin dose should include an accurate description of the distance between the X-ray beam source and the patient skin for estimates of skin dose. It should be noted that the amount of pad compression will vary at different locations on the patient, as well as for different patient weights.

Estimated standard deviations of distance errors for an SSD common to FGI procedures are shown in Table V. For example, if the assumed distance is in error from the actual distance by as much as ± 5 cm at an SSD of 60 cm, then the range of correction would be 0.85–1.15.

In this particular example, the application of a one-sided use of uncertainty may be considered as appropriate. The maximum error may be +5 cm, and not ± 5 cm, as the patient is known to be on the tabletop and pad. It is not possible for the patient skin to be closer to the X-ray tube than the tabletop. In this case, the uncertainty would be reduced accordingly.⁶⁶

Corrections for distance of the X-ray source appear straightforward when the beam transmits onto the table prior to irradiating the skin. The uncertainty for this correction factor is $\pm 5\%$.

4.A.6. Conversion of skin exposure to skin dose

The f-factor for air-tissue is commonly approximated by a value of 1.06, the accuracy will depend on tissue type and X-ray beam quality. The recent work on backscatter factors and poly-energetic mass energy-absorption coefficient ratios by Benmakhlouf et al. offers the possibility for better accuracy in f-factors.^{37–39} For most FGI procedures skin dose can be approximated by water dose with sustained accuracy.

4.A.7. Non-uniformity of the X-ray Beam

Distance corrections according to the inverse square law should be used to compute the irradiated regions of skin that are divided into patches, over the entire X-ray beam area striking the patient. However, intrinsic beam non-uniformities exist due to the heel effect, or potentially other sources such as wedge compensation filters. Furthermore, correction for backscatter is region dependent and locations in the X-ray beam that are near to the edge of the beam intercept on the patient skin will receive less scattered radiation. Any corrections to beam non-uniformities applied to the skin dose calculations should be communicated in reports on skin dose estimates.

The uncertainty imposed by the heel effect, depending on the X-ray beam quality and area striking the patient, may be up to 30%–40%.^{41,42}

4.B. Additional uncertainties involved with skin dose mapping

Skin dose mapping requires that the location of the irradiated skin is known, which means that C-arm angulation and patient position must be modelled. Specific areas on the skin irradiated during FGI procedures need to be identified for

TABLE V. Example of confidence intervals for distance uncertainties relative to an SSD of 60 cm

Assigned SSD (cm)	Estimated range of error	Estimated Range of correction factor	Estimated Standard Deviation (σ)	Estimated range of Uncertainty
60	± 2 cm	0.93 to 1.07	± 0.035	± 0.07
60	± 5 cm	0.85 to 1.15	± 0.075	± 0.15
60	± 10 cm	0.70 to 1.3	± 0.15	± 0.30

summation of dose to determine the PSD, which is the most actionable information available for follow-up of skin injury. This complex task is affected by the C-arm and X-ray beam geometry, as well as start, stop and intermediate positions of the projected beam for all irradiation events, size of skin patches, and the ability match a computational phantom (shape and positioning) to a patient. These factors all strongly affect the uncertainty of skin dose and PSD estimates. Challenging examples of skin dose mapping include irradiated regions on curved patient surfaces, slightly overlapping X-ray beams, bi-plane FGI devices, along with differences in computational phantom shape and positioning from the actual patient undergoing an FGI procedure. Table VI lists identified aspects that contribute to skin dose mapping uncertainties.

4.B.1. Computational phantoms

The Report of AAPM Task Group 246 and EFOMP for patient organ dosimetry in CT concluded that the presently known uncertainty in organ dose estimates due to computational phantoms (used in Monte Carlo simulations) depends on how accurately the chosen computational phantom resembles the anatomical structure of the actual patient and was identified as $\pm 5\%$ – 66% .³⁰ Differently from CT, however, computational phantoms in fluoroscopy use DICOM RDSR content for skin dose estimations by dividing the computational phantom surface into skin patches and referencing their positional information to the X-ray source.^{68–73} Furthermore, since the scope of this report is limited to skin dose estimation, uncertainties with choice of computational phantom is limited to the outer shape of the phantom and matching to an actual patient, which may yield lesser uncertainty compared to CT where internal organs must also be taken into account. However, as previously discussed, the presence of bone beneath the skin surface in some FGI procedures will add complexity to skin dose estimates. Also, see Section 4.B.3 on matching an individual patient with a computational phantom. More work should be done to investigate the applicability of computational phantoms to FGI device procedures.

4.B.2. Computational C-arm models

Estimates of skin dose may be derived using models of a C-arm that can represent the geometry, distance, and beam quality of an actual FGI procedure. This approach may not use the device-reported air kerma in the RDSR but rather use separate measurement(s) obtained, for example, at the isocenter. More work needs to be done to investigate C-arm models coupled with computational phantoms to identify uncertainty in irradiated regions of skin.

4.B.3. Matching a patient with a computational phantom

As this report is focused on patient skin dose, only the entrance skin surface that has been irradiated is considered in uncertainties involving matching an individual patient with a

TABLE VI. Identified uncertainties associated with skin dose mapping estimates from FGI procedures

Source	Description	Magnitude of Error
Computational Phantom Type and Format	A statement is needed on which computational phantom was used, together with characteristics: <ul style="list-style-type: none"> • Human like or cylindrical/ elliptical phantom. • Computational phantom height and weight. • Model number or another descriptor. • Size of the smallest skin patches on the phantom. 	Dependent upon phantom agreement with actual patient. If patient is supine and the X-ray tube is under the tabletop, the uncertainty may be described using Table 4.1.
Computational C-arm Models	If a virtual C-arm is used to estimate skin dose, the element matching should be stated. Further important information associated with uncertainty include: <ul style="list-style-type: none"> • SID matching to the actual FGI device. • Determination of X-ray beam shape (square or rectangular). • Longitudinal and lateral tabletop position movement for locating the X-ray beam on the phantom. 	Aspects associated with identifying the irradiated patches of the phantom skin should be noted.
Matching a Patient with a Computational Phantom	Patient size will affect accuracy of skin dose estimates, particularly with angled C-arm projections. Data on patient to phantom match should be presented.	10% to 15%
Patient Location on the Tabletop	A statement on the method used for locating the actual patient on the tabletop, for example, 15 cm from the top of the head to the end of the tabletop. Patient movement or position change during the procedure must also be taken into account.	NA
C-arm Angulation During an Irradiation Event	RDSR provide the start angle for each irradiation event, but not the stop end position. Only images sent to PACS store the C-arm angulation and tabletop locations in DICOM image header tags.	The assumptions used in the beam location on the patient should be stated. For example, all irradiation events list the start location as irradiated during an entire sequence.
Resolution of Skin Dose Regions and X-ray Beam Collimation	No agreement exists for the needed resolution.	NA

computational phantom. Most fluoroscopic procedures use the X-ray tube under the tabletop, either directly under or with angulation that still necessitates the beam to pass through the tabletop and pad, which limits the skin dose uncertainty due to patient size. For example, in any FGI procedure where the X-ray tube is directly under the patient (and tabletop), the patient size will have negligible impact on the accuracy of skin dose estimates, as the skin of a supine patient is on the pad regardless of their size. However, X-ray backscatter will be reduced with young (i.e., small) pediatric patients, and pad compression might differ with patient weight.

The uncertainty regarding the geometric difference(s) between a clinical patient and a matched computational phantom may be estimated up to $\pm 10\%$ – 15% . With X-ray tube projections under the tabletop, this uncertainty may be reduced to $\pm 3\%$ – 5% .

4.B.4. Patient location on the tabletop

Identifying the patient location on the tabletop is critical for determining the distribution of skin dose and PSD.

Various methods are available with commercial skin dose estimation software solutions, mostly concerning measurements between patient- and tabletop reference points. For example, a patient could be placed on the tabletop with the top of the head approximately 15 cm from the end of the tabletop. However, it should be noted that the skin dose mapping uncertainty would increase with distance from the patient head. The estimate of skin dose and PSD should list the method used for patient localization.

Additionally, a patient will in some cases be moved during the procedure, which may substantially affect the skin dose distribution and consequently also the PSD. If the patient is routinely moved for the type of procedure being reported, then a limitation in accuracy of the PSD for the patient positions should be noted.

4.B.5. C-arm angulation and table movement during an irradiation event

For a series of FGI images captured and transferred to a Picture Archiving and Communication System (PACS), DICOM image header tags may provide information on the

C-arm angle for each individual image. Unfortunately, very few series of images from FGI procedures are sent to PACS in clinical practice, and a last image hold (LIH) sent to PACS will only supply DICOM information on one location of a fluoroscopy irradiation event. The RDSR provides a single value for the C-arm position, but only for the first exposure of an irradiation event. Furthermore, table panning, typically performed in the cardiac catheterization lab to follow the contrast agent when it flows down the coronary arteries, would not be mapped correctly. To compute the location on the skin that has been irradiated, it may thus be necessary to assume that all irradiations were performed at the start position of a fluoroscopic event. A comparison of the start position angle of one event to the start position of the preceding (or next) event may add confidence to estimates of PSD.

For rotational C-arm acquisitions, or cone beam computed tomography (CBCT), DICOM Working Groups 2 and 28, respectively, are working on improving RDSR information.⁷⁴ Including CBCT events in skin dose and PSD estimates may be achieved with information found in anatomical protocols on FGI devices regarding incremental steps between exposures and treating a CBCT irradiation event as a regular acquisition series equally divided in multiple angulations.

4.B.6. Resolution of Skin Dose Regions and X-ray Beam Collimation

It has been discussed, for example, in Fig. 19, that subdividing the triangular elements representing the computational phantom surface can be beneficial for skin dose and PSD estimates. Very fine subdivision of elements may not improve the representation of patient curvature, but it will improve the ability to define the intersection of the X-ray beam edge, which in turn improves the resolution and separation of neighboring beams and possibly also PSD estimates.

Another uncertainty regarding resolution of skin dose regions is the X-ray beam size on the patient and approximations regarding beam collimation. If a skin dose distribution is calculated using only primary collimation, and not secondary collimation, skin dose mapping to certain skin patches potentially suffers from uncertainties of up to 100%. This may have practical consequences as high peak skin doses that would lead to patient alerts, usually occur with overlapping X-ray beams: It is therefore key to strive for a high degree of accuracy by measuring and modeling the adjustable collimator and wedge filter positions, in addition to table, C-arm and patient geometry.

5. SUMMARY OF REPORT AND RECOMMENDATIONS

The aim of the Joint Report of AAPM Task Group 357 and EFOMP was to summarize current methods and information available for the practicing medical physicist to estimate patient skin dose with FGI procedures. This endeavor was greatly aided by the continuing efforts of the scientific

medical physics community, the numerous technology enhancements and dose-controlling features provided by the FGI device manufacturers, and the emergence and greater availability of the DICOM RDSR. Refined and new dosimetry systems continue to evolve and form the infrastructure for further improvements in accuracy. Dose-related content and information systems capable of handling big data are emerging for patient dose monitoring and QA tools for large-scale multihospital enterprises. Further development of RDSR is currently undertaken by DICOM WG 28 in supplement 191: Patient Radiation Dose Reporting (P-RDSR) which will aid patient skin dose follow-up in the future.

1. The air kerma is the fundamental radiation dosimetry metric with FGI devices. It is generally a free-in-air reported value that disregards the tabletop and pad attenuation, backscatter, forward scatter, etc. Many FGI procedures with high skin dose occur with the C-arm in various angled positions, for which the accumulated air kerma does not represent patient skin dose in a meaningful way, as the patient is irradiated at multiple locations. Physical corrections, which transform air kerma to absorbed dose at the skin surface of a patient, should be applied as well as C-arm angulation and patient position correction using information, for example, from DICOM RDSR, together with appropriate computational phantoms to estimate patient skin dose.

AAPM Task Group 357 and EFOMP recommend that for all skin dose software solutions involving a computational phantom, at least one reference phantom be provided to users for which a patient in supine position with a specified location on the tabletop has a reported confidence value for a nominal 1 Gy exposure.

2. AAPM Task Group 357 and EFOMP promotes the addition of a routine QA test, according to the methods suggested by AAPM Task Group 125, to measure exposure rate to a patient whose skin is located at the PERP. This gives a better understanding of the cause of high skin doses and how to set up anatomical protocols based on FGI device AEC logic. Furthermore, FGI protocols with different skin dose rates for small, medium, and large patient sizes improve the comparative review of procedures performed with FGI devices and the comparisons of dose rates for identical procedures performed between different FGI devices.

3. Multiple sources of uncertainty in skin dose estimates have been discussed in this report. There is a knowledge gap identified by AAPM Task Group 357 and EFOMP in the literature on the magnitude of many of these uncertainties. More work should be done in general to investigate uncertainties in applied radiation dosimetry and further expand the possibilities of corrections to improve accuracy, for example, as in recent studies on collimator scatter and X-ray beam inhomogeneities.^{42,75} Furthermore, it is recommended that patient skin dose estimates should be reported together with the associated uncertainty, for example, a 95% confidence interval.

4. Skin dose estimates can be refined by using the growing number of software solutions available, both commercially and through open-source distribution. Presently available

software solutions include both skin dose mapping and real time dose monitoring, which have obvious benefits to radiation safety in FGI procedures. Regarding real time monitoring of patient skin dose during FGI procedures, it should be noted that, while such solutions might aid operators in choosing projection angles and collimation to reduce PSD, this aspect of a procedure should not get a disproportionately large degree of attention from operators: the primary task is to perform a clinically successful procedure. In addition, next to the risks of ionizing radiation, patients may be exposed to other, even greater health risks that should be addressed too. On the other hand, unnecessary caution to not exceed the thresholds for radiation injury through lack of dose information may result in premature termination of a procedure with concomitant patient health risk.

5. FGI procedures deliver real-time imaging for a wide range of clinical needs of varying complexity. Many physician specialties perform procedures on a wide range of patient sizes. These procedures are known for the variety in the physician tools (catheters, stents, glue, etc.), the targeted organ systems, and the different X-ray exposure modes, that is, fluoroscopy, DSA, and cine. AAPM Task Group 357 and EFOMP support the need for naming conventions for standardized procedures and the need to review skin dose with consideration to the procedure type and complexity, which can provide insights in the variability in patient skin dose. Along with standardized procedures, further standardization of the graphical representations, symbols and physical units that are used to express dose quantities in FGI will also facilitate the tasks and reduce practical misunderstandings. Communication of our data to clinical colleagues would be helped if standardized units and color schemes are shown at the console and in the dose map. This is especially important if facilities use FGI devices from different vendors.

6. AAPM Task Group 357 and EFOMP have identified gaps in DICOM information related to FGI procedures, which are directly relevant to the advancement of skin dose estimation. Further collaboration with MITA, FDA, IEC, and the DICOM community is crucial to advance the understanding and reporting of patient skin dose with FGI procedures.

Furthermore, AAPM Task Group 357 and EFOMP recommend that a medical physicist should verify FGI device RDSR information as part of commissioning, acceptance testing, and following software upgrades. Familiarity with RDSR information and other DICOM content, as well as software solutions for skin dose estimation, may be considered as newly added competence requirements for medical physicists involved in QA and optimization of FGI device procedures.

ACKNOWLEDGEMENTS

The authors gratefully acknowledge the input and refinements by TG357 and EFOMP consultants Stephen Balter, Sjikr Boon, Clemence Bordier, Kevin Buckley, Lionel Desponds, Ryan Fisher, James Hanson, Eric Huettl, Sofia

Kottou, Donald Miller, Richard Morin, Kevin Nelson, William O'Connell, Renato Padovani, Francisco Sureda, Stephen Vastagh, Kevin Wunderle, and Federica Zanca.

CONFLICT OF INTEREST

Jonas Andersson and Hilde Bosmans are, respectively, co-owners of companies that develop commercial dose monitoring software (Dicom Port and Qaelum).

^{a)}Author to whom correspondence should be addressed. Electronic mail: jonas.s.andersson@umu.se; Telephone: +46(0)90-785 27 96.

REFERENCES

1. U.S. Food & Drug Administration (FDA). Performance Standard for Diagnostic X-Ray Systems and Their Major Components (21CFR 1020.32); Small Entity Compliance Guide. 2007. <https://www.fda.gov/media/73941/download>. Accessed March 13, 2021.
2. Miller DL, Balter S, Cole PE, et al. Radiation doses in interventional radiology procedures: the RAD-IR study: part II: skin dose. *J Vasc Interv Radiol*. 2003;14:977–990.
3. International Electrotechnical Commission (IEC). *Medical Electrical Equipment-Part 2–43: Particular Requirements for the Basic Safety and Essential Performance of X-ray Equipment for Interventional Procedures Report 60601-2-43:2010/A2:2019*. Geneva (Switzerland): International Electrotechnical Commission; 2019.
4. Malchair F, Dabin J, Deleu M, et al. Review of skin dose calculation software in interventional radiology. *Phys Med*. 2020;80:75–83.
5. Colombo PE, Felisi M, Riga S, Torresin A. On skin dose estimation software in interventional radiology. *Phys Med*. 2021;81:182–184.
6. Greffier J, Dabli D, Frandon J, Beregi JP. Skin dose assessment in interventional radiology. *Phys Med*. 2021;81:170–172.
7. Hellström M, Granberg C, Lundman J, Åhlström Riklund K, Andersson J. Introducing PySkinDose, a novel framework for patient peak skin dose estimation in interventional radiology. ECR - EuroSafe Imaging. 2020; ESI-00814.
8. Hellström M. PySkinDose. <https://github.com/rvbCMCTS/PySkinDose>. 2019. Accessed March 13, 2021.
9. Omar A, Bujila R, Fransson A, Andreo P, Poludniowski G. A framework for organ dose estimation in x-ray angiography and interventional radiology based on dose-related data in DICOM structured reports. *Phys Med Biol*. 2016;61:3063–3083.
10. International Commission on Radiological Protection (ICRP). ICRP Publication 103: The 2007 Recommendations of the International Commission on Radiological Protection. *Ann ICRP*. 2007;37:1–332.
11. International Commission on Radiation Units and Measurements (ICRU). ICRU Report 74: Patient Dosimetry for X Rays used in Medical Imaging. ICRU, Bethesda (MD); <https://www.icru.org/report/patient-dosimetry-for-x-rays-used-in-medical-imaging-report-74/> 2005. Accessed March 13, 2021.
12. International Commission on Radiation Units and Measurements (ICRU). ICRU Report 57: Conversion Coefficients for use in Radiological Protection Against External Radiation. Bethesda (MD). Journal of the ICRU. 1998; Volume 29, Issue 2 <https://www.icru.org/report/conversion-coefficients-for-use-in-radiological-protection-against-external-radiation-report-57/>. Accessed March 13, 2021.
13. Bushberg JT, Seibert JA, Leidholdt EMJ, Boone JM. *The Essential Physics of Medical Imaging*. 3rd edn. Philadelphia: Lippincott, Williams and Wilkins; 2012.
14. Lin P-J, Schueler BA, Balter S, et al. Accuracy and calibration of integrated radiation output indicators in diagnostic radiology: a report of the AAPM Imaging Physics Committee Task Group 190. *Med Phys*. 2015;42:6815–6829.
15. International Electrotechnical Commission (IEC). *Medical electrical equipment-Part 2–43: Particular Requirements for the Basic Safety and*

- Essential Performance of X-ray Equipment for Interventional Procedures Report 60601-2-43*, 2nd edn. Geneva (Switzerland): IEC; 2010.
16. International Electrotechnical Commission (IEC). 60601-1-3:2008 Medical electrical equipment - Part 1-3: General requirements for basic safety and essential performance - Collateral standard: Radiation protection in diagnostic X-ray equipment, 2nd Edition. Geneva (Switzerland): IEC; 2008.
 17. American Association of Physicists in Medicine (AAPM). Report of AAPM Task Group 125. Functionality and Operation of Fluoroscopic Automatic Brightness Control/Automatic Dose Rate Control Logic in Modern Cardiovascular and Interventional Angiography Systems. AAPM 2012. https://www.aapm.org/pubs/reports/RPT_125.pdf. Accessed March 13, 2021.
 18. Gislason-Lee AJ, McMillan C, Cowen AR, Davies AG. Dose optimization in cardiac x-ray imaging. *Med Phys*. 2013;40:091911.
 19. Gislason-Lee AJ, Davies AG, Cowen AR. Dose optimization in pediatric cardiac x-ray imaging. *Med Phys*. 2010;37:5258–5269.
 20. deBlois F, Landry G, Verhaegen F. SpekCalc. 2007. <http://spekcalc.weebly.com/>. Accessed March 13, 2021.
 21. Bujila R, Omar A, Poludniowski G. A validation of SpekPy: a software toolkit for modelling X-ray tube spectra. *Phys Med*. 2020;75:44–54.
 22. Bujila R, Omar A, Poludniowski G. SpekPy. https://bitbucket.org/spekpy/spekpy_release/wiki/Home. Accessed March 13, 2021.
 23. Turner AC, Zhang DI, Kim HJ, et al. A method to generate equivalent energy spectra and filtration models based on measurement for multidetector CT Monte Carlo dosimetry simulations. *Med Phys*. 2009;36:2154–2164.
 24. FDA guidelines. "Performance Standard for Diagnostic X-Ray Systems and Their Major Components (21CFR 1020.30, 1020.31, 1020.32, 1020.33). Small Entity Compliance Guide," (Silver Springs, MD); 2007.
 25. National Electrical Manufacturers Association (NEMA). *NEMA XR 31-2016 Standard Attributes on X-ray Equipment for Interventional Procedures: MITA Smart dose Interventional Technology*. Arlington (VA): NEMA; 2016. <http://www.nema.org/Standards/Pages/Standard-Attribute-s-on-X-ray-Equipment-for-Interventional-Procedures.aspx>. Accessed March 13, 2021.
 26. Sobol WT. High frequency x-ray generator basics. *Med Phys*. 2002;29:132–144.
 27. Lin PJ. The operation logic of automatic dose control of fluoroscopy system in conjunction with spectral shaping filters. *Med Phys*. 2007;34:3169–3172.
 28. Aufrechtig R, Xue P, Thomas CW, et al. Perceptual comparison of pulsed and continuous fluoroscopy. *Med Phys*. 1994;21:245–256.
 29. Khodadadegan Y, Zhang M, Pavlicek W, et al. Validation and initial clinical use of automatic peak skin dose localization with fluoroscopic and interventional procedures. *Radiology*. 2013;266:246–255.
 30. American Association of Physicists in Medicine (AAPM). Report of AAPM Task Group 246 and EFOMP. Estimating Patient Organ Dose with Computed Tomography: A Review of Present Methodology and Required DICOM Information. AAPM; 2019. https://www.aapm.org/pubs/reports/RPT_246.pdf. Accessed March 13, 2021.
 31. International Commission on Radiation Units and Measurements (ICRU). Key data for ionizing-radiation dosimetry: measurement standards and applications. ICRU Report 90. Bethesda (MD). Journal of the ICRU, 2014: 1–118. <https://www.icru.org/report/icru-report-90-key-data-for-ionizing-radiation-dosimetry-measurement-standards-and-applications/>. Accessed March 13, 2021.
 32. International Atomic Energy Agency (IAEA). Technical Reports Series no 457: Dosimetry in diagnostic radiology: An international code of practice. 2007. https://www-pub.iaea.org/MTCD/publications/PDF/TRS457_web.pdf. Accessed March 13, 2021.
 33. Attix FH. *Introduction to radiological physics and radiation dosimetry*. New York: John Wiley & Sons; 2008.
 34. Berger MJ, Coursey JS, Zucker MA. ESTAR, PSTAR, and ASTAR: Computer programs for calculating stopping-power and range tables for electrons, protons, and helium ions. NIST; 1999. <https://www.nist.gov/publications/estar-pstar-and-astar-computer-programs-calculating-stopping-power-and-range-tables-0>. Accessed March 13, 2021.
 35. Petoussi-Hens N, Zankl M, Drexler G, Panzer W, Regulla D. Calculation of backscatter factors for diagnostic radiology using Monte Carlo methods. *Phys Med Biol*. 1998;43:2237–2250.
 36. Harrison RM. Backscatter factors for diagnostic radiology (1–4 mm Al HVL). *Phys Med Biol*. 1982;27:1465–1474.
 37. Benmakhlof H, Bouchard H, Fransson A, Andreo P. Backscatter factors and mass energy-absorption coefficient ratios for diagnostic radiology dosimetry. *Phys Med Biol*. 2011;56:7179–7204.
 38. Benmakhlof H, Fransson A, Andreo P. Influence of phantom thickness and material on the backscatter factors for diagnostic x-ray beam dosimetry. *Phys Med Biol*. 2013;58:247–260.
 39. Benmakhlof H, Fransson A, Andreo P. Backscatter factors and mass energy-absorption coefficient ratios for surface dose determination in diagnostic radiology Report KS-ASF-201101-IR. Stockholm 2011. https://www.researchgate.net/publication/282814112_2011_Benmakhlof_Fransson_Andreo_BSF_mu_en_diag_radiol_dosimetry_Report_KS-ASF-201101-IR. Accessed March 13, 2021.
 40. Colombo PE, Rottoli F, Felisi M, et al. Validation of a dose tracking software for skin dose map calculation in interventional radiology. *Phys Med*. 2020;72:122–132.
 41. Rana VK. A dose tracking system for real-time feedback to the physician during image-guided neurointerventional procedures using a biplane X-Ray imaging system. PhD Dissertation. UB Proquest Database. 2014.
 42. Wunderle KA, Godley AR, Shen ZL, Dong FF. Technical Note: Characterization of x-ray beam profiles for a fluoroscopic system incorporating copper filtration. *Med Phys*. 2019;46:4918–4922.
 43. Anderson JA, Wang J, Clarke GD. Choice of phantom material and test protocols to determine radiation exposure rates for fluoroscopy. *Radiographics*. 2000;20:1033–1042.
 44. Compagnone G, Pagan L, Bergamini C. Comparison of six phantoms for entrance skin dose evaluation in 11 standard X-ray examinations. *J Appl Clin Med Phys*. 2005;6:101–113.
 45. Ma CM, Seuntjens JP. Mass-energy absorption coefficient and backscatter factor ratios for kilovoltage x-ray beams. *Phys Med Biol*. 1999;44:131–143.
 46. Omar A, Benmakhlof H, Marteinsdottir M, Bujila R, Nowik P, Andreo P. Monte Carlo investigation of backscatter factors for skin dose determination in interventional neuroradiology procedures. *Proc SPIE Int Soc Opt Eng*. 2014;9033:2042159.
 47. Hubbell JH, Seltzer SM. NIST Standard Reference Database 126, Tables of X-Ray Mass Attenuation Coefficients and Mass Energy-Absorption Coefficients from 1 keV to 20 MeV for Elements Z = 1 to 92 and 48 Additional Substances of Dosimetric Interest. NIST; 2004.
 48. Seuntjens JP, Thierens H, Van der Plaetsen A, Segaert O. Conversion factor f for X-ray beam qualities, specified by peak tube potential and HVL value. *Phys Med Biol*. 1987;32:595–603.
 49. Schauer DA, Seltzer SM, Links JM. Exposure-to-absorbed-dose conversion for human adult cortical bone. *Appl Radiat Isot*. 1993;44:485–489.
 50. Vijayan S, Xiong Z, Guo C, et al. Calculation of Forward Scatter Dose Distribution at the skin entrance from the patient table for fluoroscopically guided interventions using a pencil beam convolution kernel. *Proc SPIE Int Soc Opt Eng*. 2018;10573:2294920.
 51. DeLorenzo MC, Goode AR. Evaluation of skin dose calculation factors in interventional fluoroscopy. *J Appl Clin Med Phys*. 2019;20:159–168.
 52. Johnson PB, Borrego D, Balter S, Johnson K, Siragusa D, Bolch WE. Skin dose mapping for fluoroscopically guided interventions. *Med Phys*. 2011;38:5490–5499.
 53. Bednarek DR, Barbarits J, Rana VK, Nagaraja SP, Josan MS, Rudin S. Verification of the performance accuracy of a real-time skin-dose tracking system for interventional fluoroscopic procedures. *Proc SPIE Int Soc Opt Eng*. 2011;7961: 877677.
 54. Rana VK, Rudin S, Bednarek DR. Updates in the real-time dose tracking system (DTS) to improve the accuracy in calculating the radiation dose to patients skin during fluoroscopic procedures. *Proc SPIE Int Soc Opt Eng*. 2013;8668. <https://doi.org/10.1117/12.2007706>.
 55. Digital Imaging and Communications in Medicine (DICOM) Standards Committee, Working Group 2. Digital Imaging and Communications in Medicine (DICOM) Supplement 83: Enhanced XA Image Storage SOP Class/ Enhanced XRF Image Storage SOP Class. Rosslyn (Virginia) 2005. <https://www.dicomstandard.org/News-dir/ftsups/docs/sups/sup83.pdf>. Accessed March 13, 2021.

56. National Electrical Manufacturers Association (NEMA). DICOM PS3.3 2021a - Information Object Definitions, C.8.7.5 XA Positioner Module, C.8.7 X-Ray Modules. Arlington 2016. <http://dicom.nema.org/medical/dicom/2016c/output/pdf/part03.pdf>. Accessed March 13, 2021.
57. den Boer A, de Feijter PJ, Serruys PW, Roelandt JR. Real-time quantification and display of skin radiation during coronary angiography and intervention. *Circulation*. 2001;104:1779–1784.
58. Bordier C, Klausz R, Desponds L. Patient dose map indications on interventional X-ray systems and validation with Gafchromic XR-RV3 film. *Radiat Prot Dosimetry*. 2015;163:306–318.
59. Bastioni M. MakeHuman. 2016. <http://makehumancommunity.org/>. Accessed March 13, 2021.
60. Foundation Blender, Blender. 2004–2016. <https://www.blender.org/foundation/>.
61. Sunday D. Line and Intersection Plane. <http://geomalgorithms.com/a06-intersect-2.html>. Accessed March 13, 2021.
62. SAE International. Digitally defining the human body. <https://www.sae.org/standardsdev/tsb/cooperative/caesar.htm>. Accessed March 13, 2021.
63. Rana VK, Rudin S, Bednarek DR. Improved-resolution real-time skin-dose mapping for interventional fluoroscopic procedures. *Proc SPIE Int Soc Opt Eng*. 2014;19:9033.
64. Vijayan S, Rana VK, Rudin S, Bednarek DR. Incorporating corrections for the head-holder and compensation filter when calculating skin dose during fluoroscopically-guided interventions. *Proc SPIE Int Soc Opt Eng*. 2015;9412.
65. Wilson SM, Prasan AM, Viridi A, et al. Real-time colour pictorial radiation monitoring during coronary angiography: effect on patient peak skin and total dose during coronary angiography. *EuroIntervention*. 2016;12:e939–e947.
66. Bureau International des Poids et Mesures, and Joint Committee for Guides in Metrology. Evaluation of measurement data - Guide to the expression of uncertainty in measurement. 2008. https://www.bipm.org/utis/common/documents/jcgm/JCGM_100_2008_E.pdf. Accessed March 13, 2021.
67. Jones AK, Ensor JE, Pasciak AS. How accurately can the peak skin dose in fluoroscopy be determined using indirect dose metrics? *Med Phys*. 2014;41:071913.
68. Farah J, Broggio D, Franck D. Creation and use of adjustable 3D phantoms: application for the lung monitoring of female workers. *Health Phys*. 2010;99:649–661.
69. Farah J, Broggio D, Franck D. Female workers and in vivo lung monitoring: a simple model for morphological dependence of counting efficiency curves. *Phys Med Biol*. 2010;55:7377–7395.
70. Farah J, Broggio D, Franck D. Examples of Mesh and NURBS modelling for in vivo lung counting studies. *Radiat Prot Dosimetry*. 2011;144:344–348.
71. Christ A, Kainz W, Hahn EG, et al. The Virtual Family—development of surface-based anatomical models of two adults and two children for dosimetric simulations. *Phys Med Biol*. 2010;55:N23–38.
72. Lee C, Lodwick D, Hasenauer D, Williams JL, Lee C, Bolch WE. Hybrid computational phantoms of the male and female newborn patient: NURBS-based whole-body models. *Phys Med Biol*. 2007;52:3309–3333.
73. Lee C, Lodwick D, Williams JL, Bolch WE. Hybrid computational phantoms of the 15-year male and female adolescent: applications to CT organ dosimetry for patients of variable morphometry. *Med Phys*. 2008;35:2366–2382.
74. National Electrical Manufacturers Association (NEMA), Working Group 02 and 28. Supplement 214: Cone Beam CT RDSR. The document is in letter ballot. <https://www.dicomstandard.org/news-dir/current/docs/sups/sup214-slides.pdf>. Accessed March 13, 2021.
75. Tao AT, Miller D, Hindal M, Fetterly KA. Technical Note: assessment of scatter originating from the x-ray tube collimator assembly of modern angiography systems. *Med Phys*. 2019;46:4371–4380.